

1

Power Amplifier Fundamentals

1.1 Introduction

A power amplifier (PA) is an essential component, playing a key role in the realization of many microwave and millimetre-wave systems. PA applications span a broad range of areas [1], among which telecommunications, radar [2–4], electronic warfare, heating [5, 6], and medical microwave imaging [7–12] represent just a few examples. Given such extremely diversified fields, PA specifications may greatly differ in operating, technological and design requirements. As a consequence, a wide variety of PA realizations results, from travelling-wave tube amplifiers in satellite payloads to solid-state amplifiers for personal wireless communication handsets, from microwave heating tubes to amplifiers composing hyperthermia apparatus.

Regardless of its physical realization, the task of a PA is to increase the power level of the signal at its input in a given frequency band, up to a predefined level at its output. As contrasted therefore to low-level (i.e. linear) amplifiers, often specified in term of small-signal gain, the absolute output power level, as well as the power gain, become the PA's primary performance.

The need for high output power levels is the main driver in the selection of the active devices composing the PA, on the basis of their output power capabilities. Moreover, to limit the power consumption, active devices are typically operated under large-signal regimes, so fully swinging their nonlinear characteristics. Otherwise, a sufficiently large active device could be adopted, resulting in an almost linear behaviour, while dissipating a large amount of DC power for voltage and current biasing.

A PA is therefore to be considered as a nonlinear system component, whose large-signal operating conditions often lead to detrimental effects on the output signal, resulting in a distorted replica of the input. On the other hand, the linear approximation underlying small-signal amplifier design techniques is no longer strictly valid, hence not allowing their direct application to PA design. Dedicated methodologies have to be exploited and adopted, even if preliminary and first guess approaches can be employed.

PA design is typically the result of a trade-off, trying to fulfil several conflicting requirements such as linearity vs. efficiency or high output power level vs. low distortion. The design approach to be selected depends on operating frequency and bandwidth, available device technology, application (fixed, mobile or satellite communications, modulated CW or pulsed signal, etc.) and many other factors [13].

2 HIGH EFFICIENCY SOLID STATE POWER AMPLIFIERS

1.2 Definition of Power Amplifier Parameters

In a PA, the **output power** P_{out} is the power delivered to the external load (usually 50 ohm) at a specified frequency f or in a frequency band $B = [f_{Low}, f_{High}]$, expressed as:

$$P_{out} = P_{out}(f) = \frac{1}{2} \operatorname{Re} \{ V_{out} \cdot I_{out}^* \} \quad f \in [f_{Low}, f_{High}] \quad (1.1)$$

while the **input power** P_{in} is the available input power at the same frequency, i.e.

$$P_{in} = P_{in,av}(f) = \frac{1}{2} \operatorname{Re} \{ V_{in} \cdot I_{in}^* \} \quad f \in [f_{Low}, f_{High}] \quad (1.2)$$

The PA **power gain** G is defined as the ratio between output and input power:

$$G(f) = \frac{P_{out}(f)}{P_{in}(f)} \quad f \in [f_{Low}, f_{High}] \quad (1.3)$$

The power gain, due to the nonlinear behaviour of the devices used in the PA, clearly depends on the input signal level. However, for very small drive levels, the amplifier behaves almost linearly, and it is usually possible to refer to this linear gain G_L , defined as:

$$G_L(f) = \lim_{P_{in} \rightarrow 0} [G(f)] \quad f \in [f_{Low}, f_{High}] \quad (1.4)$$

On the contrary, when the input drive is increased, output current and voltage swings allowed by the active device tend to be limited by its nonlinearities. Thus output power tends to saturate to the value

$$P_{sat}(f) = \lim_{P_{in} \rightarrow \infty} [P_{out}(f)] \quad f \in [f_{Low}, f_{High}] \quad (1.5)$$

with the corresponding power gain approaching zero

$$\lim_{P_{in} \rightarrow \infty} [G(f)] = 0 \quad f \in [f_{Low}, f_{High}] \quad (1.6)$$

A typical plot of the active device output current and voltage waveforms, for an increasing input power level P_{in} , is reported in Fig. 1.1.

Assuming a non-zero quiescent bias current and increasing the input power, both output current and voltage waveforms change from a sinusoidal shape to a distorted one, as a result of the device nonlinearities.

Due to the broad dynamic range of the signals involved in a PA, power quantities are usually expressed in logarithmic units. In particular, assuming 1 mW as a reference, power levels are expressed in decibels over 1 mW, i.e. in dBm:

$$P_{dBm} = 10 \cdot \log_{10} \left(\frac{P}{1 \text{ mW}} \right) = 10 \cdot \log_{10}(P_{mW}) = 10 \cdot \log_{10}(P_W) + 30 \quad (1.7)$$

$$P_{mW} = 10^{\frac{P_{dBm}}{10}}$$

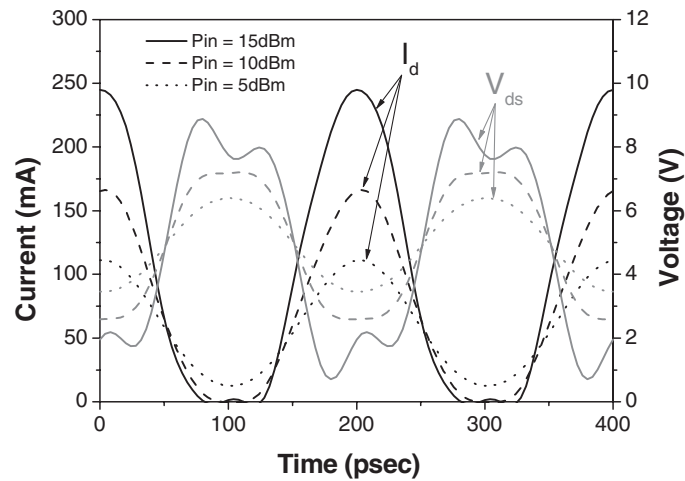


Figure 1.1 Example of active device output current and voltage waveforms for three different input power levels P_{in} .

Similarly, for the power gain the logarithmic scale is adopted, defining

$$G_{dB} = 10 \cdot \log_{10}(G) = P_{out,dBm} - P_{in,dBm} \quad (1.8)$$

Output power and power gain are graphically represented as functions of the input power (while performing a *power sweep*) using logarithmic scales. In particular, with the input power expressed in dBm on the abscissa, output power in dBm or the power gain in dB is reported on the y-axis, as illustrated in Fig. 1.2.

The power sweep in Fig. 1.2 reveals that the power gain decreases from its linear value G_L (small signal regime) down to $-\infty$ in dB scale (i.e. 0 in linear scale). Such behaviour, due to nonlinear

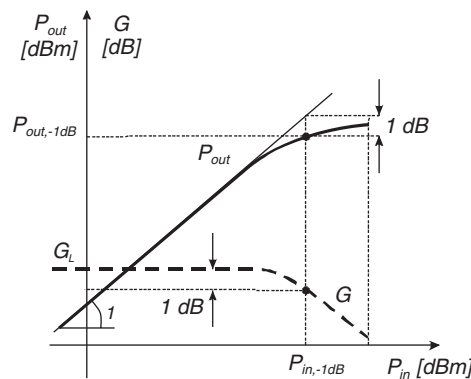


Figure 1.2 Sample $P_{in} - P_{out}$ power sweep (continuous line) and corresponding amplifier power gain G (dashed line). From both P_{-1dB} can be derived.

4 HIGH EFFICIENCY SOLID STATE POWER AMPLIFIERS

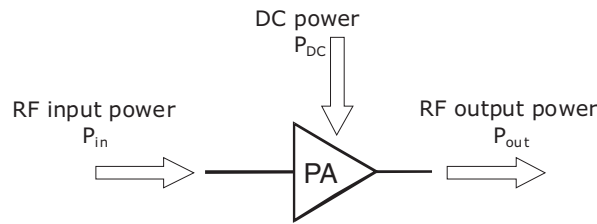


Figure 1.3 Energetic schematic representation of PA operation.

phenomena in the large signal regime, is referred to as *gain compression*. In some cases, and in particular for some bias conditions, an eventual gain expansion from G_L can be observed before a gain compression is experienced. A widely used figure-of-merit for the compression behaviour, namely the *-1dB compression point* $P_{out, -1dB}$, is defined as the output power level corresponding to a 1 dB deviation from the ideal linear behaviour (see Fig. 1.2). The corresponding input power level, $P_{in, -1dB}$, is used to mark the border between ‘highly nonlinear’ and ‘almost linear’ drive level regions. Input $P_{in, -1dB}$ and output $P_{out, -1dB}$ powers are clearly related through the linear power gain G_L by:

$$P_{out, -1dB} = (G_{L, dB} - 1) \cdot P_{in, -1dB} \quad (1.9)$$

It is however possible to define (and determine) the power levels corresponding to any gain compression level, as required by the particular application (e.g. in pulsed radar or saturated power operations, where up to 2 or 3 dB gain compression is required).

From the energetic point of view, and regardless of the specific application, a PA may be ultimately regarded as a component converting DC power from supplies (P_{DC}) into microwave power (i.e. P_{out}). This process is schematically illustrated in Fig. 1.3, where, if a voltage supply is assumed,

$$P_{DC} = V_{bias} \cdot \frac{1}{T} \cdot \int_0^T I_{bias}(t) \cdot dt \quad (1.10)$$

The effectiveness of this conversion process is usually measured by means of the amplifier’s *efficiency*, η , defined as the ratio between output RF and supplied DC power:

$$\eta \triangleq \frac{P_{out}}{P_{DC}} \quad (1.11)$$

Efficiency is often further specified as *drain efficiency* (η_d) or *collector efficiency* (η_c) in the case of a solid-state PA based on field-effect or bipolar transistors, respectively.

The amplifier’s efficiency is indeed one of the key parameters in specifying overall system performance: for a given output power requested to the PA, efficiency actually determines the DC power budget and hence the supply power. A reduced supply power resulting from high efficiency performance is a key goal of mobile apparatus, typically battery-operated, whose operating time strictly depends on the transmitting section power requests.

Since practical and physical constraints impose an actual efficiency lower than the 100% theoretical maximum,¹ high efficiency performance implies in turn a low power dissipated on the power-amplifying

¹ Assuming an ideal active device without leakage currents and paths.

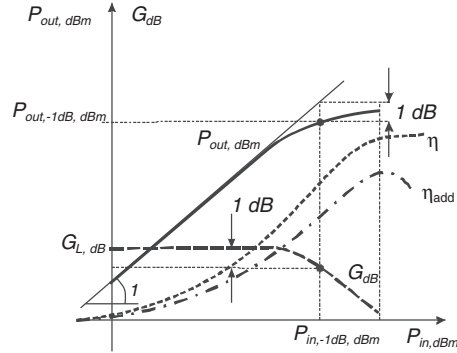


Figure 1.4 Typical performance in a PA as a function of input drive.

device, therefore reducing actual size and weight of the heat sinks eventually required. On the other hand, for a given available DC power, a high efficiency performance allows higher transmitted power with a corresponding increase in overall system capabilities.

The efficiency is usually expressed as a percentage, i.e.

$$\eta_{\%} = 100 \cdot \eta \quad (1.12)$$

and it is usually reported on the same plot together with power and gain, as shown in Fig. 1.4. In such a plot the efficiency is exponentially dependent on the input power reported on the abscissa, since

$$\eta = \frac{P_{out}}{P_{DC}} = \frac{G \cdot P_{in}}{P_{DC}} = \frac{G}{1000 \cdot P_{DC}} \cdot 10^{\frac{P_{in,dBm}}{10}} \quad (1.13)$$

Therefore, at least in the linear region, where G remains constant and thus independent of P_{in} , efficiency increases exponentially while increasing the input drive. If P_{in} is further increased, due to the gain compression phenomena related to the nonlinear active device behaviour, both gain G and DC power P_{DC} start depending on P_{in} , and efficiency usually tends to saturate to a maximum value, as depicted in Fig. 1.4.

As frequency increases, however, the PA gain decreases, as a result of its active constituents gain roll-off behaviour. The contribution to the output power coming directly from the input drive cannot therefore be neglected, since it constitutes, at microwave frequencies and beyond, a significant portion of the total. As a consequence, the *added power*, P_{add} , i.e. the net increase in the signal power from the PA input to its output, is defined as:

$$P_{add} \triangleq P_{out} - P_{in} = P_{out} \cdot \left(1 - \frac{1}{G}\right) \quad (1.14)$$

A more meaningful parameter, the *Power-Added Efficiency* (PAE or η_{add} are the typically adopted symbols) is therefore defined as the ratio between the added power and the supplied DC power:

$$\eta_{add} \triangleq \frac{P_{add}}{P_{DC}} = \frac{P_{out} - P_{in}}{P_{DC}} = \frac{P_{out} \cdot \left(1 - \frac{1}{G}\right)}{P_{DC}} = \eta \cdot \left(1 - \frac{1}{G}\right) \quad (1.15)$$

6 HIGH EFFICIENCY SOLID STATE POWER AMPLIFIERS

An alternative definition of η_{add} , less frequently used in common practice, is [14]:

$$\eta_{add} \triangleq \frac{P_{out}}{P_{DC} + P_{in}} = \eta \cdot \frac{1}{1 + \frac{\eta}{G}} \quad (1.16)$$

expressing the ratio of output power to the total input power (*RF* plus *DC*, see Fig. 1.3) to the amplifier.

The two definitions practically converge for high-gain amplifiers, while giving substantially different results for low-gain amplifiers, especially when hardly driven into compression (note that the conventional definition of η_{add} may lead to negative values in hard compression).

Regardless of the adopted definition for η_{add} , its maximization is to be achieved at the nominal drive level for the PA, i.e. while the latter is delivering the desired output power. In such operating conditions, the amplifier is typically driven into compression, thus leaving its almost linear region and approaching the nonlinear active device physical limitations, as depicted in Fig. 1.4, where the typical swept power performance of a PA is reported.

The peak drain/collector or power-added efficiency usually occurs at high drive levels, corresponding to 2–4 dB gain compression: in this region the active device behaviour is therefore highly nonlinear and correspondingly design methodologies for high efficiency operation must cope with such an intrinsic deviation from linearity.

If non-constant envelope signals have to be handled by the PA, an *average efficiency* can be introduced [13–15], defined as in (1.11), where the quantities in the expression are replaced by input and output powers averaged over an envelope period and weighted by the envelope probability density function (PDF), i.e.

$$\eta_{AVG} = \frac{P_{out,AVG}}{P_{DC,AVG}} = \frac{\frac{1}{T} \int_0^T P_{out}(t) \cdot PDF(t) \cdot dt}{\frac{1}{T} \int_0^T P_{DC}(t) \cdot PDF(t) \cdot dt} \quad (1.17)$$

For cascaded amplifying stages, as depicted in Fig. 1.5, the overall efficiency η_{tot} is easily computed by:

$$\eta_{tot} = \frac{P_{out}}{P_{DC,1} + P_{DC,2}} = \frac{\eta_2}{1 + \frac{P_{DC,1}}{P_{DC,2}}} = \frac{\eta_2}{1 + \frac{\eta_2}{\eta_1 \cdot G_2}} \quad (1.18)$$

Since the *DC* supply power for final stages ($P_{DC,2}$) is usually much larger than the driver supply ($P_{DC,1}$), overall efficiency is dominated from the former amplifier. On the contrary, for a low-gain final amplifier, also the driver's effect becomes crucial for overall conversion efficiency.

The conversion from *DC* to *RF* power implies that a fraction of the supplied power is lost and actually dissipated on the active power device. The major part of such loss is located at the active device

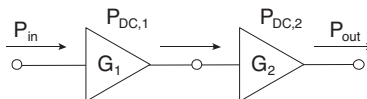


Figure 1.5 Cascade connection of two PAs.

output, and is given by:

$$P_{diss,out} \triangleq \frac{1}{T} \cdot \int_T v(t) \cdot i(t) \cdot dt \quad (1.19)$$

$v(t)$ and $i(t)$ being the device output voltage and current, integrated over a period (T) of the RF signal. To increase conversion efficiency, to be discussed later, a possible strategy consists in the minimization of such dissipated power, i.e. in the proper shaping of device output voltage and current waveforms.

It is possible to relate the power dissipated in the active device output to the power added efficiency. In fact, assuming that such dissipated power is the portion of the DC supplied power not contributing to the added power, then

$$P_{diss,out} = P_{DC} - P_{add} = P_{DC} - P_{out} + P_{in} \quad (1.20)$$

In the case of a reasonably high gain, it is easy to get

$$P_{diss,out} = P_{out} \cdot \left[\frac{(1 - \eta_{add}) - \frac{(1 - \eta_{add})}{G}}{\eta_{add}} \right] \approx P_{out} \cdot \left(\frac{1}{\eta_{add}} - 1 \right) \quad (1.21)$$

Thus a higher power added efficiency implies a lower power dissipation in the active device, with major effects in reducing thermal issues and increasing device lifetime.

1.3 Distortion Parameters

As previously described, efficiency and output power of a PA are limited by compression and saturation, due to nonlinear phenomena. Such a nonlinear behaviour clearly introduces a distortion on the output voltage and current waveforms, thus degrading the signal quality and consequently the information content to be transmitted, often beyond acceptable levels. In particular, and especially in communication systems featured by non-constant envelope signals (as in the case of QAM or in digital cellular communications with GSM and NADC standards), the transmitter has to fulfil tight requirements not only in terms of efficiency but also regarding linearity and spectral purity.

The nonlinear behaviour (i.e. the distortion) must therefore be properly classified and evaluated as a further PA figure of merit.

Several indicators of PA linearity or deviation from linearity are used, depending on the system specifications and modulation schemes that are to be adopted.

In order to introduce and define such indicators, a simple third-order approximation of the PA transfer characteristic is usually adopted, i.e.

$$y(t) = k_1 \cdot x(t) + k_2 \cdot x^2(t) + k_3 \cdot x^3(t) \quad (1.22)$$

where $x(t)$ and $y(t)$ are the input and output signal to the amplifier, respectively (normalized voltages or currents, measured in \sqrt{W}), k_1 is the small-signal voltage (or current) gain, and k_2 , k_3 are the first two coefficients of a McLaurin series expansion of the PA transfer characteristic, truncated to third order.

Please note that the above approximation, relating the output signal to the instantaneous input value, actually describes a memoryless system, and therefore memory effects cannot be accounted for in this

8 HIGH EFFICIENCY SOLID STATE POWER AMPLIFIERS

description. Moreover, in this case the coefficient k_1 , k_2 and k_3 correspond to the first three orders of Volterra kernels, which will be discussed in chapter 3 [16, 17].

If a single-tone excitation is assumed for the input signal, with amplitude X and frequency f , i.e.

$$x(t) = X \cdot \cos(2\pi f \cdot t) = X \cdot \cos(\omega \cdot t) = \frac{X}{2}(e^{j\omega t} + e^{-j\omega t}) \quad (1.23)$$

The corresponding input power P_{in} (on a unitary normalizing resistor) is:

$$P_{in} = \frac{X^2}{2} \quad (1.24)$$

The output signal, according to (1.22), becomes:

$$y(t) = X \cdot \left(k_1 + \frac{3}{4} k_3 \cdot X^2 \right) \cdot \cos(\omega \cdot t) + k_2 \cdot \frac{X^2}{2} + k_2 \cdot \frac{X^2}{2} \cdot \cos(2\omega \cdot t) + k_3 \cdot \frac{X^3}{4} \cdot \cos(3\omega \cdot t) \quad (1.25)$$

Thus the output power at frequency f , $P_{out,f}$, and large-signal gain G , are obtained as

$$\begin{aligned} P_{out,f} &= \frac{1}{2} \cdot \left[X \cdot \left(k_1 + \frac{3}{4} k_3 \cdot X^2 \right) \right]^2 = k_1^2 \cdot \left(1 + \frac{3}{2} \cdot \frac{k_3}{k_1} \cdot P_{in} \right)^2 \cdot P_{in} \\ &= G_L \cdot \left(1 + \frac{3}{2} \cdot \frac{k_3}{k_1} \cdot P_{in} \right)^2 \cdot P_{in} \end{aligned} \quad (1.26)$$

$$G = \frac{P_{out,f}}{P_{in}} = G_L \cdot \left(1 + \frac{3}{2} \cdot \frac{k_3}{k_1} \cdot P_{in} \right)^2 \quad (1.27)$$

It can be noted from (1.26) that the term $3k_3/2k_1$ represents a gain compression factor if negative, or an expansion factor if positive, as depicted in Fig. 1.6.

Since usually k_3/k_1 is negative, the previous derivation accounts for large-signal gain compression, i.e. decrease from the ideal constant value (G_L).

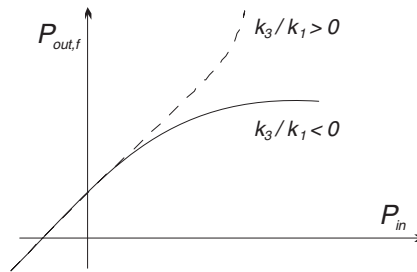


Figure 1.6 $P_{out,f}$ vs. P_{in} for $k_3/k_1 < 0$ (gain compression, continuous line) or $k_3/k_1 > 0$ (expansion, dashed).

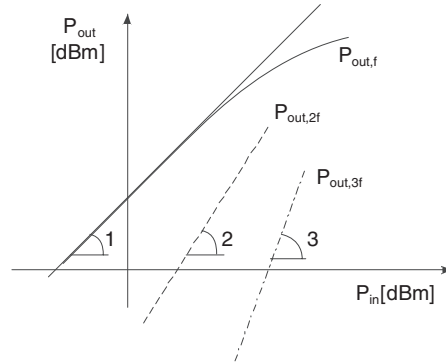


Figure 1.7 Output power in a single-tone test at fundamental frequency (continuous), second (dash) and third (dash-dot) harmonic components.

In the same way, from the single-tone excitation, harmonic generation at $2f$ and $3f$ arises, leading to corresponding output power generated at harmonic frequencies $P_{out,2f}$ and $P_{out,3f}$, given by:

$$P_{out,2f} = \frac{1}{2} \left(k_2 \cdot \frac{X^2}{2} \right)^2 = \frac{1}{2} G_L \left(\frac{k_2}{k_1} \right)^2 \cdot P_{in}^2 \quad (1.28)$$

$$P_{out,3f} = \frac{1}{2} \left(k_3 \cdot \frac{X^3}{4} \right)^2 = \frac{1}{4} G_L \left(\frac{k_3}{k_1} \right)^2 \cdot P_{in}^3$$

therefore justifying the increase in harmonic power by n dB per dB increase in input power, n being the harmonic order under consideration, as depicted in Fig. 1.7.

In general, for moderate excitations, i.e. for small amplitudes of the input level P_{in} , but sufficient to generate harmonic distortion, the output power delivered at the generic harmonic frequency nf , is proportional to the n -th power of P_{in} , i.e.

$$P_{out,nf} \propto (P_{in})^n \quad \Leftrightarrow \quad P_{out,nf,dBm} \propto n \cdot P_{in,dBm} \quad (1.29)$$

1.3.1 Harmonic Distortion

The *harmonic distortion* due to the n -th output harmonic component, HD_{nf} , is defined in a straightforward manner by:

$$HD_{nf} \triangleq \frac{P_{out,nf}}{P_{out,f}} \quad (1.30)$$

resulting in the approximated expressions for second and third harmonic distortion (HD_{2f} , HD_{3f}) that is easily derived via the simple cubic memoryless model:

$$HD_{2f} = \frac{1}{2} \left(\frac{k_2}{k_1} \right)^2 \cdot P_{in} \quad (1.31)$$

$$HD_{3f} = \frac{1}{4} \left(\frac{k_3}{k_1} \right)^2 \cdot P_{in}^2$$

10 HIGH EFFICIENCY SOLID STATE POWER AMPLIFIERS

Similarly, a total harmonic distortion (*THD*) is defined summing up all harmonic distortion components in the output signal as:

$$THD \triangleq \sum_{n \geq 2} \frac{P_{out,nf}}{P_{out,f}} \quad (1.32)$$

The above quantities are typically expressed in logarithmic units (decibels) over the carrier power (dBc).

1.3.2 AM-AM/AM-PM

As previously stated, the model adopted in (1.22) is an instantaneous one, i.e. a memoryless description of the PA input-output characteristics. Real-world amplifiers are indeed dynamic systems with memory, whose nonlinear behaviour affects also the phase of the output signal. In fact, if the input signal to the PA is assumed to be:

$$x(t) = X(t) \cdot \cos[2\pi f \cdot t + \varphi(t)] \quad (1.33)$$

its output may exhibit nonlinear phenomena both in amplitude and phase:

$$y(t) = G[X(t)] \cdot \cos\{2\pi f \cdot t + \varphi(t) + \Phi[X(t)]\} \quad (1.34)$$

giving rise to the AM/AM compression and AM/PM conversion effects, described by a nonlinear relationship between input and output amplitudes representing the amplifier's output power compression and a change in phase depending on the input signal drive level:

$$\begin{aligned} G[X(t)] &\neq k \cdot X(t) \\ \Phi[X(t)] &\neq const \end{aligned} \quad (1.35)$$

Typical AM/AM compression and AM/PM conversion plots are reported in Fig. 1.8. In particular, the AM/PM conversion effect represents a change in the phase of the output that depends on the input drive level. This effect is potentially dangerous not only in communication systems, giving rise for instance to distorted QAM constellations, but also in phased array applications, where the phase of each signal exiting the respective PA actually determines the active antenna beam pointing.

1.3.3 Two-tone Intermodulation

The information gathered via a single-tone test however may not suffice in many cases, since usually the input signals to the PA are modulated rather than single-tone, thus resulting in a populated spectrum over a frequency band. If the input stimulus is a narrowband signal, it can be represented either as a carrier modulated by a relatively slow envelope or as a summation of finite and closely spaced tones within the bandwidth. Other figures are therefore adopted to characterize the nonlinear PA behaviour starting with a simple two-tone test.

Resorting to the memoryless PA model, a two-tone test may be performed, trying in this way to simulate the simultaneous treatment of two different signals and therefore their mutual interaction in the nonlinear PA. Much in the same way, this test may give an insight on a broadband signal, whose components (the tones in the test) may interfere leading to a distorted output. This is clearly an approximation since the two signals are in reality much more complex than simple sinusoids; on the

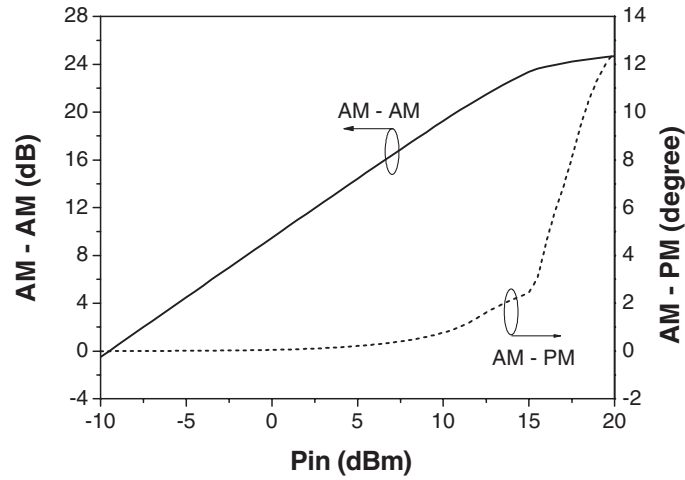


Figure 1.8 Typical AM/AM compression and AM/PM conversion curves for a PA.

other hand the two-tone test is simple enough to be easily carried out experimentally. The input signal in this case is given by two closely spaced tones at frequencies f_1 and f_2 ($f_1 < f_2$) with amplitudes X_1 and X_2 respectively:

$$\begin{aligned} x(t) &= X_1 \cdot \cos(2\pi f_1 \cdot t) + X_2 \cdot \cos(2\pi f_2 \cdot t) \\ &= X_1 \cdot \cos(\omega_1 \cdot t) + X_2 \cdot \cos(\omega_2 \cdot t) \end{aligned} \quad (1.36)$$

In the two-tone test, frequency spacing ($f_2 - f_1$) is much lower than single component frequencies, to replicate a narrowband excitation. Moreover, a close spacing may help in considering the PA gain as almost constant at the two frequencies.

By inserting such an input drive into the PA truncated expansion in (1.22), the output signal becomes:

$$\begin{aligned} y(t) &= \frac{k_2}{2} X_1^2 + \frac{k_2}{2} X_2^2 + \\ &+ X_1 \cdot \left[k_1 + \frac{3}{4} k_3 X_1^2 + \frac{3}{2} k_3 X_2^2 \right] \cos(\omega_1 \cdot t) + \\ &+ X_2 \cdot \left[k_1 + \frac{3}{4} k_3 X_2^2 + \frac{3}{2} k_3 X_1^2 \right] \cos(\omega_2 \cdot t) + \\ &+ X_1^2 \frac{k_2}{2} \cdot \cos(2\omega_1 \cdot t) + X_2^2 \frac{k_2}{2} \cdot \cos(2\omega_2 \cdot t) + \\ &+ X_1 X_2 k_2 \cdot \{ \cos[(\omega_2 - \omega_1) \cdot t] + \cos[(\omega_2 + \omega_1) \cdot t] \} + \\ &+ X_1^3 \frac{k_3}{4} \cdot \cos(3\omega_1 \cdot t) + X_2^3 \frac{k_3}{4} \cdot \cos(3\omega_2 \cdot t) + \\ &+ \frac{3}{4} k_3 X_1^2 X_2 \cdot \{ \cos[(2\omega_1 + \omega_2) \cdot t] + \cos[(2\omega_1 - \omega_2) \cdot t] \} + \\ &+ \frac{3}{4} k_3 X_1 X_2^2 \cdot \{ \cos[(2\omega_2 + \omega_1) \cdot t] + \cos[(2\omega_2 - \omega_1) \cdot t] \} \end{aligned} \quad (1.37)$$

12 HIGH EFFICIENCY SOLID STATE POWER AMPLIFIERS

Table 1.1 Output components in a two-tone test grouped by the originating term in the truncated series expansion.

Originating Term	Output Frequencies	Corresponding Amplitude	Nomenclature
$x(t)$	f_1, f_2	X_1, X_2	Linear term
	$2 \cdot f_1, 2 \cdot f_2$	X_1^2, X_2^2	Second harmonic
	dc (from f_1), dc (from f_2)	X_1^2, X_2^2	Rectified component
$x^2(t)$	$f_1 - f_2$	$X_1 \cdot X_2$	Second-order intermodulation
	$f_1 + f_2$	$X_1 \cdot X_2$	Second-order intermodulation
	f_1, f_2	X_1^3, X_2^3	Compression
$x^3(t)$	f_1, f_2	$X_1 \cdot X_2^2, X_1^2 \cdot X_2$	Suppression
	$3 \cdot f_1, 3 \cdot f_2$	X_1^3, X_2^3	Third harmonic
	$2 \cdot f_1 - f_2, 2 \cdot f_2 - f_1$	$X_1^2 \cdot X_2, X_1 \cdot X_2^2$	Third-order intermodulation
	$2 \cdot f_1 + f_2, 2 \cdot f_2 + f_1$	$X_1^2 \cdot X_2, X_1 \cdot X_2^2$	Third-order intermodulation

In general, n th-order intermodulation components, for n odd, will have coefficients given by

$$\frac{1}{2^{n-1}} \cdot \binom{n}{\frac{n+1}{2}} \cdot k_n \cdot X^n \tag{1.38}$$

Thus, several output frequency components result, summarized in Table 1.1, and grouped by the term in the expansion (linear, quadratic or cubic) originating them.

The terms in Table 1.1 are plotted as a function of frequency in Fig. 1.9.

From Table 1.1 and Fig. 1.9, a series of considerations can be drawn. Firstly, the interaction between the two input frequencies does create, in the nonlinear PA, a series of frequency components that are not present if the PA is separately excited by the single frequencies. In fact, while DC, harmonic components and compression terms are already generated from the single-tone excitation, intermodulation frequencies and suppression terms are not. The latter contributions, giving rise to out-of-band and in-band components, actually exhibit a power level increase by 3 dB per dB increase of the single tones' power (see Table 1.1). In particular, the suppression term (often referred to as the *capture* term) tends to decrease the power output at a given fundamental frequency (say f_1) proportionally to the square of the

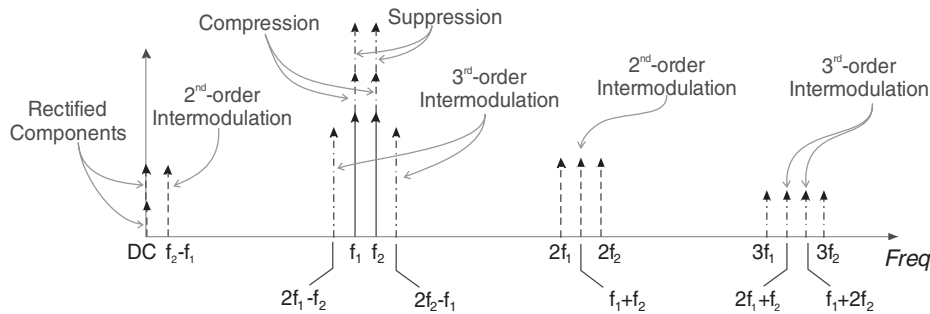


Figure 1.9 Frequency allocation of the output components originated in a two-tone test.

power of the other (f_2) fundamental frequency; this phenomenon is particularly dangerous at high drive levels, and may eventually lead to the cancellation of one of the signal components at the PA output, thus justifying the *suppression* denomination.

Moreover, if signal purity is concerned, harmonic contributions (at DC, second and third harmonic of each input excitation) together with second-order intermodulation and the terms at $2f_2 + f_1$ and $2f_2 + f_1$ fall far away from the useful part of the output signal (at f_1 and f_2), and are therefore eliminated by filtering (see Fig. 1.9). Other contributions, closer in frequency to the desired input replica, cannot be filtered out: from the simple derivation performed above, they consist in two terms located at $2f_2 - f_1$ and $2f_1 - f_2$ (commonly referred to as *third-order intermodulation components*, giving rise to *Intermodulation Distortion, IMD*) and at the input signal frequencies f_1 and f_2 (*in-band distortion*, given by the compression and suppression terms):

$$IMD \triangleq P_{out}(2f_{2n(2m)} - f_{m(n)}) \quad n, m = 1, 2 \quad (1.39)$$

1.3.4 Intercept Point IPn

Considering one of the two third-order intermodulation components and simultaneously sweeping the input tones' power, the *third-order intercept point (IP3)* is defined as the output ($IP3_{out}$) or input ($IP3_{in}$) power level at which the third-order IMD component level equals the ideal linear output power of the PA. Such a definition is graphically illustrated in Fig. 1.10.

Even if both useful output signal and IMD powers tend to saturate for some input drive, the IP3 definition consists in the ideal extrapolation of both output signal components, ideally rising by 1 dB and 3 dB per dB increase in input power respectively, and in the search for their intercept (the IP3). On the basis of such a graphical arrangement, it is clear that the resulting input drive level ($IP3_{in}$ in Fig. 1.10) is well into the PA nonlinear operating region and it is far beyond typical operating drives for a PA.

If we resort to the adopted power-series expansion, it can be shown (see appendix) that the IP3 output power level ($IP3_{out}$) can be related to the single-tone 1-dB compression point ($P_{out,1T,-1dB}$) by:

$$IP3_{out} \approx P_{out,1T,-1dB} + 10.6 \text{ dB} \quad (1.40)$$

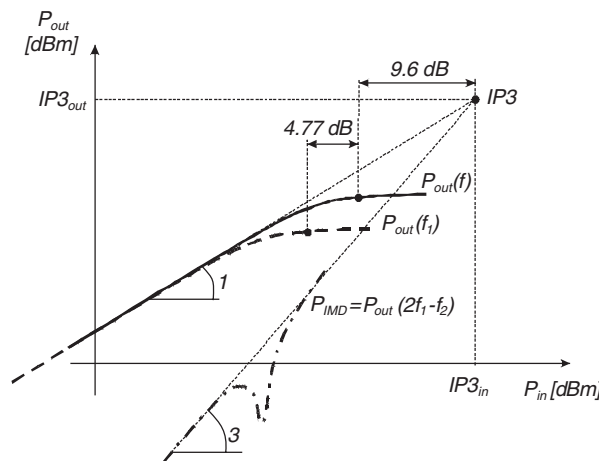


Figure 1.10 Third-order intercept point definition.

14 HIGH EFFICIENCY SOLID STATE POWER AMPLIFIERS

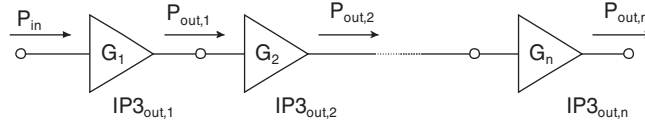


Figure 1.11 Cascade of power stages.

and similarly that the output power at 1dB compression point in the presence of two tones ($P_{out,2T,-1dB}$) is related to the same quantity obtained with the single-tone test ($P_{out,1T,-1dB}$) by:

$$P_{out,1T,-1dB} \approx P_{out,2T,-1dB} + 4.77 \text{ dB} \quad (1.41)$$

Similar intercept points can be defined (even if seldom used) by extension for higher-order intermodulation products, such as $IP5$ (for fifth-order distortion, located at $3f_2 - 2f_1$) or $IP7$ (for seventh-order distortion, located at $4f_2 - 3f_1$).

In real-world PAs, the expressions above typically overestimate $IP3_{out}$ by 2~3 dB. The approximation inherent in the truncated expansion adopted in (1.22) is in fact valid in a limited range of input drive levels, that is typically violated in the $IP3$ region. For such large drive levels, fifth and higher order contributions arise and significantly modify the results of the simplified approach.

In any case, once the PA $IP3_{out}$ is known, the actual IMD level relative to the output signal level may be found from:

$$P_{IMD} = 3 \cdot P_{out,dBm} - 2 \cdot IP3_{out} \quad (1.42)$$

As power amplifiers can be made by several cascaded stages, it is interesting to get a simple formula to relate the total $IP3$ for a structure like that depicted in Fig. 1.11.

It can be demonstrated that the total $IP3$ can be written as:

$$IP3_{out,TOT} = \frac{1}{\frac{1}{IP3_{out,1}} + \frac{G_1}{IP3_{out,2}} + \frac{G_1 G_2}{IP3_{out,3}} + \dots + \frac{G_1 G_2 \dots G_{n-1}}{IP3_{out,n}}} \quad (1.43)$$

1.3.5 Carrier to Intermodulation Ratio

Another frequently adopted indicator of the PA nonlinear behaviour is the C/I or carrier-to-intermodulation ratio, defined as the ratio between useful output power and IMD output power. It is usually measured, using logarithmic units, in decibels below the carrier (dBc):

$$C/I \triangleq \frac{P_{out}}{P_{IMD}} \quad (1.44)$$

In real-world amplifiers, due to several reasons among which matching network components and memory effects, output powers at the two fundamental frequencies and the third order intermodulation products in the upper and lower sidebands, can be different [18, 19]. This effect leads to four possible ways to define and measure the C/I figure

$$C/I \triangleq \frac{P_{out}[f_n(m)]}{P_{out}[2f_{2n(2m)} - f_{m(n)}]} \quad n, m = 1, 2 \quad (1.45)$$

Such a C/I is clearly dependent on the input power to the PA, and it decreases by 2 dB per dB increase of the input drive. Combining the two relationships above, we have in fact:

$$\left(C/I\right)_{dBc} = 2 \cdot (IP3_{out} - P_{out,dBm}) \quad (1.46)$$

1.3.6 Spurious Free Dynamic Range

For moderate drive levels (say up to 10 dB below $P_{out,-1dB}$), the third-order intermodulation term is the dominant distortion mechanism. It is therefore possible to define a linearity range for the PA as the range of input drive levels for which P_{IMD} remains below the noise floor (noise output power) of the amplifier. Such a linearity range is usually indicated as the *Spurious-Free Dynamic Range (SFDR)*, graphically reported in Fig. 1.12.

From the knowledge of the PA Noise Factor F (or Noise Figure NF in dB), its bandwidth B and (available) gain G , the *SFDR* can be computed. In fact, the available output noise power from the amplifier is given by:

$$N_{out} = kT_0 \cdot B \cdot G \cdot F \rightarrow N_{out,dBm} = B_{dBHz} + G_{dB} + NF - 174dB \quad (1.47)$$

From the leftmost part of Fig. 1.12, noting the slopes of the IMD and output power lines, we can derive:

$$SFDR_{dB} = \frac{2}{3} \cdot (IP3_{out,dBm} - N_{out,dBm}) \quad (1.48)$$

and therefore finally

$$SFDR_{dB} = \frac{2}{3} \cdot [IP3_{out,dBm} - NF_{dB} - G_{dB} - B_{dBHz} + 174 dB] \quad (1.49)$$

1.3.7 Adjacent Channel Power Ratio

The figures of merit defined above for linearity evaluation are related to single- or two-tone tests, trying to mimic in this way the PA behaviour in response to narrowband or multi-carrier input. Real-world input signals to a PA may deviate substantially from the single-tone approximation, since modulation formats and bandwidth occupation may differ significantly.

In order to account for signal distortion and the related spectral regrowth in the case of band-limited input signals, an *Adjacent Channel Power Ratio (ACPR)* is introduced.

With reference to Fig. 1.13, several definitions are adopted for such an indicator: the most commonly used refers to the *Total ACPR (ACPR_{TOT})*, i.e. the ratio between the total output power in the signal

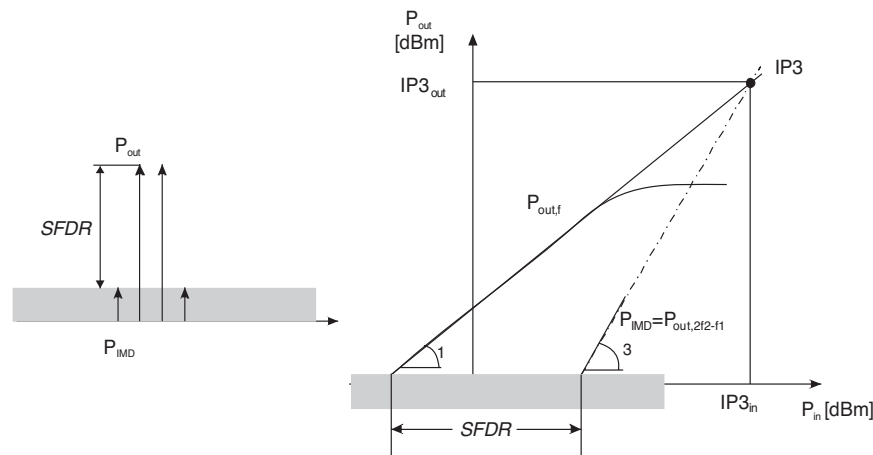


Figure 1.12 Definition of the spurious-free dynamic range.

16 HIGH EFFICIENCY SOLID STATE POWER AMPLIFIERS

bandwidth and the total output power in adjacent channels:

$$ACPR_{TOT} \triangleq \frac{P_{in-band}}{P_{adjacent-channels}} = \frac{\int_B P_{out}(f) \cdot df}{\int_{LS} P_{out}(f) \cdot df + \int_{US} P_{out}(f) \cdot df} \quad (1.50)$$

Clearly, if a single sideband is concerned, a *Lower-Sideband ACPR* ($ACPR_{LS}$) or *Upper-Sideband ACPR* ($ACPR_{US}$) can be defined, using the proper adjacent channel power in the definition:

$$ACPR_{LS} \triangleq \frac{\int_B P_{out}(f) \cdot df}{\int_{LS} P_{out}(f) \cdot df} \quad (1.51)$$

$$ACPR_{US} \triangleq \frac{\int_B P_{out}(f) \cdot df}{\int_{US} P_{out}(f) \cdot df} \quad (1.52)$$

Moreover, a *Spot ACPR* ($ACPR_{SPOT}$) is introduced, utilizing the adjacent channel power contained in a predefined bandwidth (B_x) at a given *offset* (see Fig. 1.13), defined by:

$$ACPR_{SPOT} \triangleq \frac{\int_B P_{out}(f) \cdot df}{\int_{B_x, offset} P_{out}(f) \cdot df} \quad (1.53)$$

The various ACPR figures clearly provide a deeper insight into the distortion properties of a PA if compared to their single- or two-tone counterpart, being related to a specific band-limited input signal. Nevertheless, if the input signal is approximated by a number of equally-spaced equal-amplitude tones, closed-form relationships may be found between the figures [20–22].

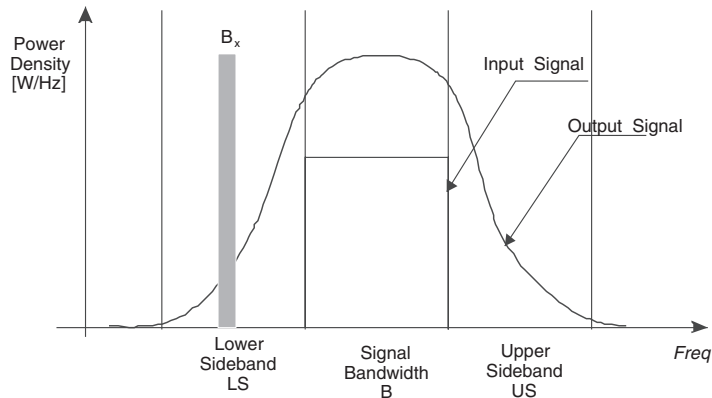


Figure 1.13 Input and output power spectral densities for adjacent channel power ratio definitions.

1.3.8 Noise and Co-Channel Power Ratio (NPR and CCPR)

Other indicators of PA linearity requiring appropriate tests are the Noise Power Ratio (NPR) and Co-Channel Power Ratio (CCPR). Both figures were proposed as an indirect characterization of the co-channel distortion [21, 23].

The former (NPR) is based on the idea of measuring the distortion due to co-channel carriers eliminating the fundamental signal in the portion of spectrum where the test is to be made, to avoid its dominant perturbation to the sought IMD signals.

Referring to Fig. 1.14, the test bench is composed by a (noise) source generating a white spectrum in the amplifier bandwidth. Such an exciting signal is then passed through a very narrowband (notch) filter, with a bandpass width ω_N centred at the frequency ω_0 to be characterized. If $\omega_N \ll \omega_0$, then a required measuring window is created without affecting the test conditions. Such a modified signal is then fed into the amplifier (or in general into the device under test, DUT) and the output spectrum is observed. In this way, any power density observed within the notch position, i.e. in the band ω_N around ω_0 , can be ascribed to the spectral regrowth phenomena due to the nonlinear behaviour of the amplifier under test.

The noise power ratio is therefore defined as:

$$NPR(\omega_0, \omega_N) \triangleq \frac{P_{out}(\omega_0 \pm \frac{\omega_N}{2})}{P_{out}(\omega_0)} \quad (1.54)$$

P_{out} being the output power density. Such a figure is usually expressed in a logarithmic scale (dB).

It is possible to relate the NPR to the ACPR if a uniformly distributed noise power over the channel is assumed, resulting in [22, 24]:

$$ACPR = -NPR - 10 \cdot \log \frac{\text{channel bandwidth}}{\text{notch bandwidth}} = -NPR - 10 \cdot \log \frac{\omega_C}{\omega_N} \quad (1.55)$$

where ω_C is the bandwidth of the adjacent channel considered in the measurement.

The Co-channel Power Ratio (CCPR) characterization is quite similar to the NPR test. Differently from the latter, the generated fundamental signals are not deleted from the input but directly at the output of the amplifier under test. In this way, the nonlinear effects introduced by the DUT at the fundamental frequency ω_0 and affecting the adjacent channels are properly considered in the measurements of the power at the adjacent channel (i.e. $\omega_0 \pm \omega_N/2$).

The proposed characterization set-up, useful also for NPR measurements, is reported in Fig. 1.15, with the corresponding spectra reported in Fig. 1.16 [25, 26].

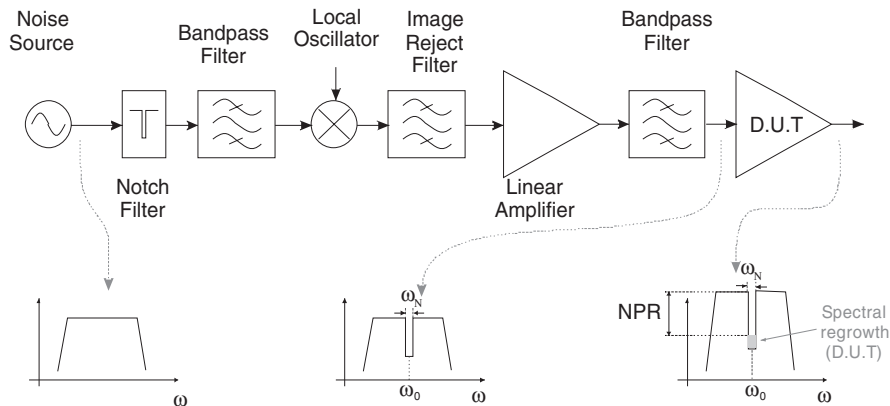


Figure 1.14 Noise power ratio definition and characterizing set-up.

18 HIGH EFFICIENCY SOLID STATE POWER AMPLIFIERS

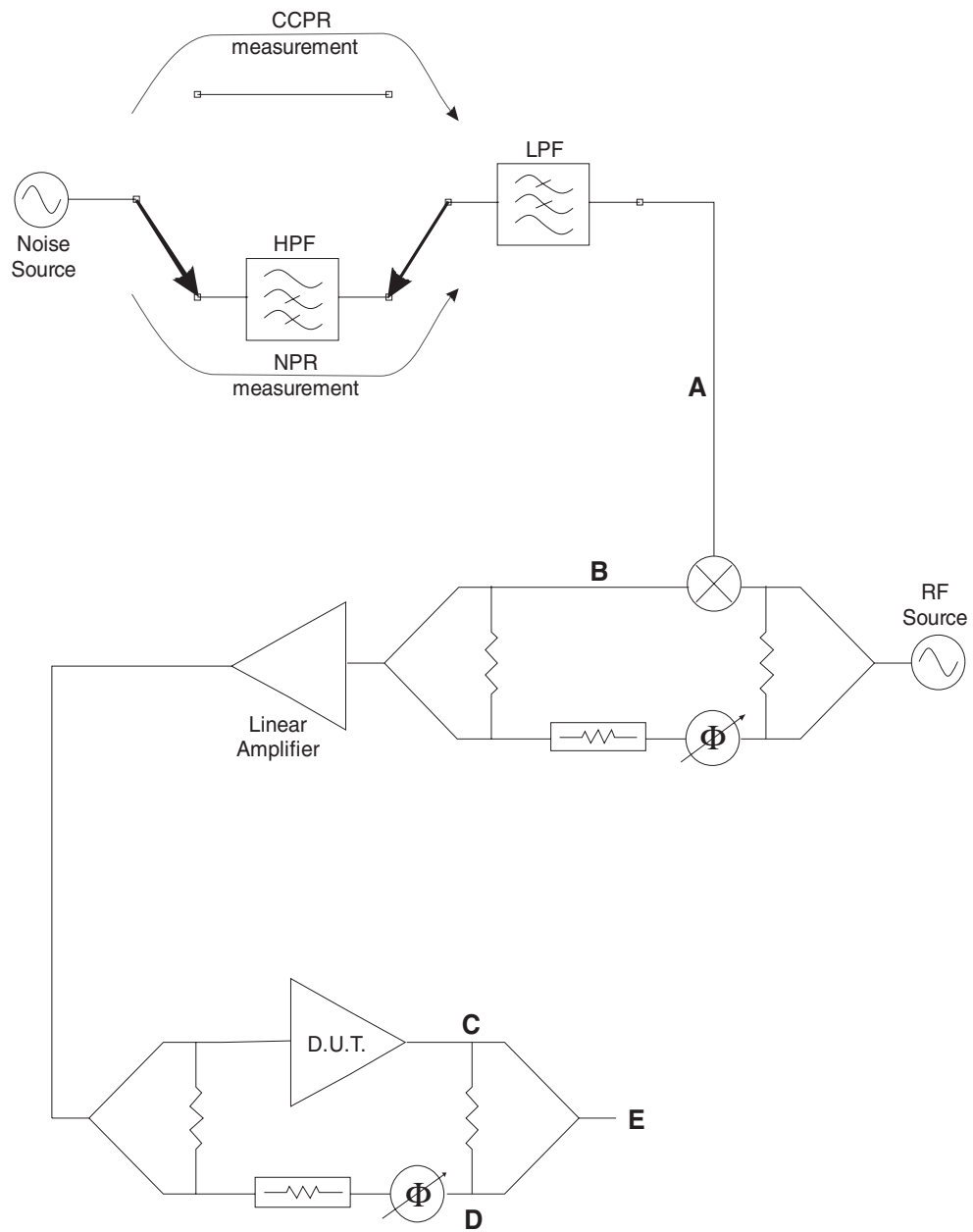


Figure 1.15 Characterization set-up for NPR and CCPR [25, 26].

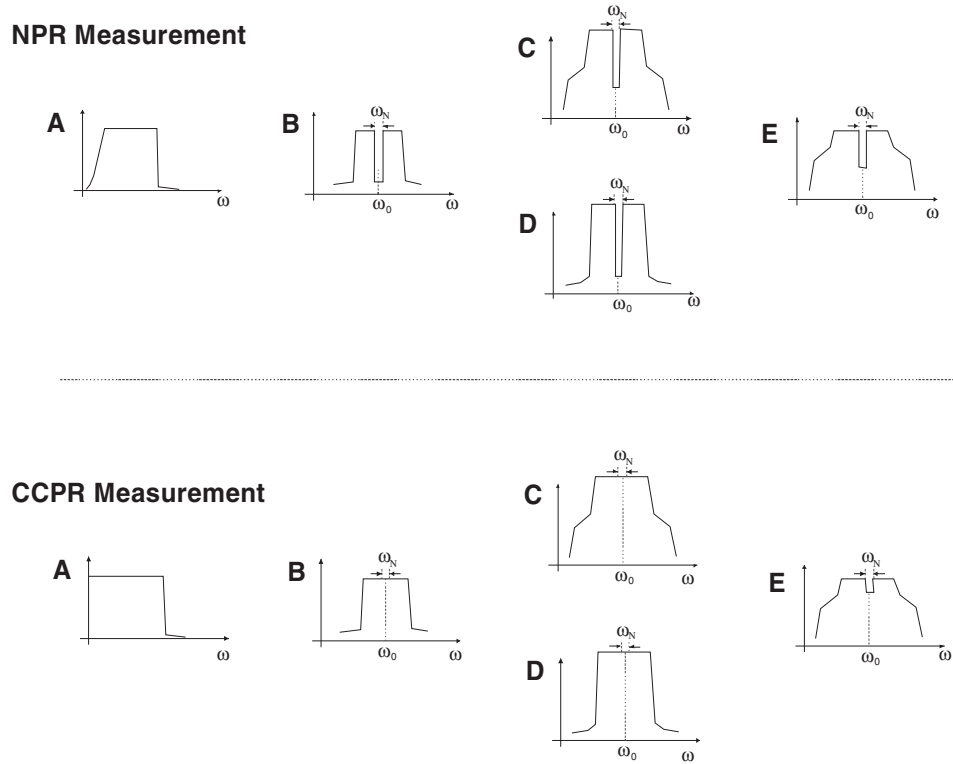


Figure 1.16 Spectra arising from the set-up depicted in Fig. 1.16.

The CCPR can be therefore defined much in the same way as the NPR, while accounting for the different test set-up:

$$CCPR(\omega_0, \omega_N) \triangleq \frac{P_{out}\left(\omega_0 \pm \frac{\omega_N}{2}\right)}{P_{out}(\omega_0)} \quad (1.56)$$

1.3.9 Multi-tone Intermodulation Ratio

The two-tone test is usually far away from the actual operating conditions of a PA, while also excessively stressing its behaviour, being equivalent to a modulated input signal with an infinite value for the peak to minimum power ratio. For this reason, another figure of merit has been proposed, the Multitone Intermodulation Ratio (*M-IMR*) [20]: it is defined as the ratio between the measured output power at the desired (i.e. under test) tone at frequency ω_0 , and the power measured at the generic tone located at frequency ω_T , as schematically depicted in Fig. 1.17

$$M-IMR(\omega_0, \omega_T) \triangleq \frac{P_{out}(\omega_0)}{P_{out}(\omega_T)} \quad (1.57)$$

This figure is usually expressed in dB.

20 HIGH EFFICIENCY SOLID STATE POWER AMPLIFIERS

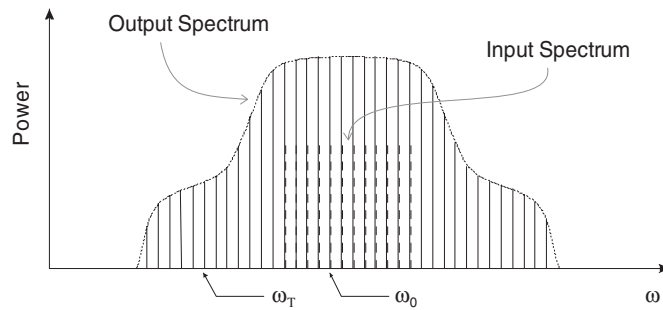


Figure 1.17 Multitone intermodulation ratio definition.

1.3.10 Error Vector Magnitude

The Error Vector Magnitude (EVM) is an additional figure adopted to quantify the distortion produced by a nonlinear amplifier (or an entire transmission chain): it actually measures the modulation fidelity of digital signals. The EVM is extracted from the constellation plots, providing the magnitude of the distortion of digital signal distribution at the sampling instants. It is defined as the difference between an ideal reference waveform and the measured one, as depicted in Fig. 1.18.

A series of definitions of EVM has actually been introduced, all of them focusing on such an error vector [27].

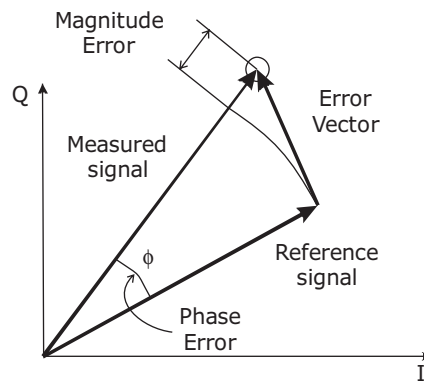


Figure 1.18 Error vector magnitude and related quantities.

1.4 Power Match Condition

Power limiting mechanisms in active devices reside in their inherent physical constraints. For a FET device, and referring to the active device output IV characteristics reported in Fig. 1.19, the limitations arise in both limited voltage and current swings. For the current, the saturation is related to the input junction forward conduction (a) and device channel pinch-off (b). Similarly, for the voltage swing, the

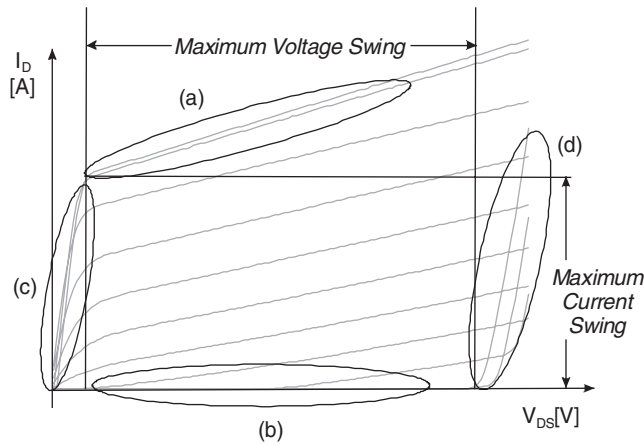


Figure 1.19 Example of device output IV characteristics and physical limitations on output current and voltage swings.

limitation is related to the ohmic behaviour (c) and breakdown (d), both channel and gate-drain junction related.

Collectively, such constraints pose an upper limit to the maximum swings that output current and voltage may experience, reflecting in a corresponding limit to the device output power generation capabilities.

As briefly outlined in the introduction, a PA is a nonlinear system, whose design requires suitable and specialized methodologies, if compared to small-signal (linear) amplifiers (gain or low-noise). The latter in fact are based on well-established techniques. After the active device is selected together with its operating (bias) point, from the knowledge of the device scattering parameters and depending on the amplifier specifications, input and output matching networks specifications (i.e. the impedances to be presented at the device input and output ports) are readily obtained via closed-form expressions [28–30]. On the contrary, for a power amplifier the S-parameter representation loses its validity due to the inherently large signal operating conditions.

However, assuming a simplified device model, as depicted in Fig. 1.20, it is possible to infer some simple and effective considerations. The device output is represented by a controlled current source (controlled by the input voltage if a FET is considered) shunted by its output small-signal admittance (represented by an output conductance g_{ds} and capacitance C_{ds}).

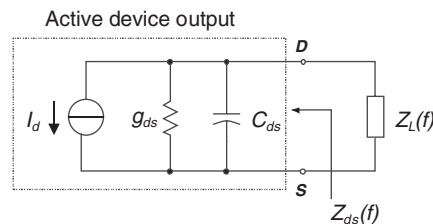


Figure 1.20 Schematic representation of the active device output connected to an external load Z_L .

22 HIGH EFFICIENCY SOLID STATE POWER AMPLIFIERS

The condition usually imposed for maximum power transfer from the device output to the external load, compatibly with device stability, is the well-known conjugate matching

$$Z_L(f) = Z_{ds}^*(f) \quad \Leftrightarrow \quad \begin{cases} G_L(f) = g_{ds} \\ B_L(f) = -j\omega \cdot C_{ds} \end{cases} \quad (1.58)$$

where

$$Z_L(f) = G_L(f) + j \cdot B_L(f) \quad (1.59)$$

$$Z_{ds}(f) = G_{ds}(f) + j \cdot B_{ds}(f) = g_{ds} + j\omega \cdot C_{ds} \quad (1.60)$$

The conjugate matching condition therefore implies the compensation of the active device output reactive part and a match in its small-signal output conductance, thus ensuring at the same time the maximization of the amplifier small-signal gain.

As a result, the corresponding load line (i.e. the curve describing the relationship between current and voltage) on the device output characteristics becomes the curve **A** reported in Fig. 1.21.

If the same condition is adopted driving the amplifier to operate into the large-signal regime, a reduced current swing results, producing in turn a sudden compression of the device output power (voltage-limited operation). On the other hand, if the external load is selected in order to fully exploit the maximum current swing, as curve **B** in Fig. 1.21, a reduced voltage swing is produced (current-limited operation), again driving the active device output into compression. The optimum situation is clearly in the simultaneous maximization of current and voltage swings, resulting in curve **C** in Fig. 1.21, often referred to as a *load-line matching condition* or *power match condition* [13]. The output power corresponding to the three situations described in Fig. 1.21 is reported in Fig. 1.22 as a function of the input drive.

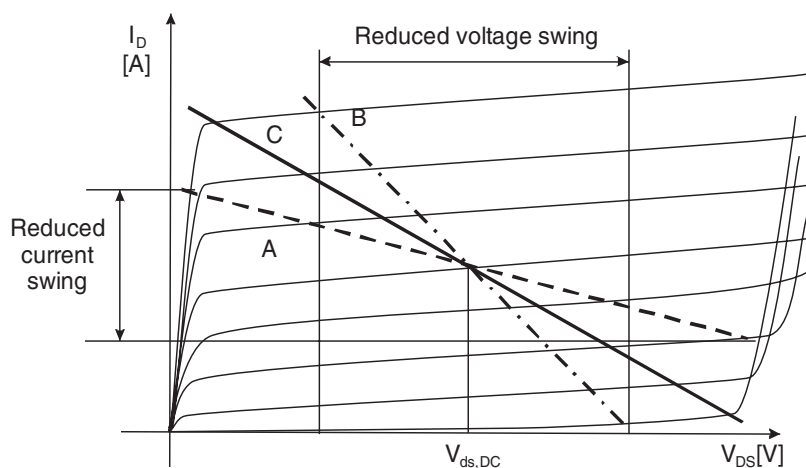


Figure 1.21 Active device output characteristics with superimposed the conjugate-match load line (A), voltage-limited (B) and optimum Loading (C).

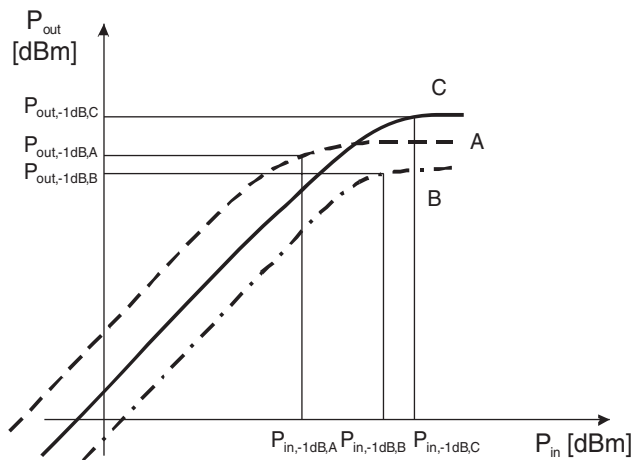


Figure 1.22 Output power for three loading conditions of Fig. 1.21: voltage-limited (A), current-limited (B), optimum loading (C).

Nevertheless, PAs that are load-line matched exhibit poor output VSWR in the system in which they are adopted. If necessary, this problem can be solved through the use of output isolators or transformers (clearly decreasing output power and efficiency by their losses) or resorting to balanced configurations if possible, as will be described in chapter 10. However, also in this case combining structure losses actually affect overall power performance.

1.5 Class of Operation

PAs are normally classified on the basis of their *operating classes*. Such a traditional classification, which may seem natural and simple at first glance, may on the contrary be ambiguous and misleading. With the term operating class in fact, several different features can be referred to, ranging from the bias point selection (Class A, AB, B or C), to the selection of matching network topologies (Tuned Load, Class F, etc.) or to the operating conditions of the active device (Class E, Class S, etc.).

In order to avoid confusion, in this book the term *biasing class* (i.e. Class A, AB, B or C) will be adopted to define the active device quiescent bias adopted in the design of the PA. However, also in this case, a clearer picture is needed to avoid confusing classifications.

In fact, the identification of the quiescent bias point may be performed in terms of device output conduction angle (CCA) Φ , i.e. the fraction of the RF signal period where a non-zero current is flowing. Alternatively, it is assumed in terms of the current value as compared to the maximum allowable one, i.e. the ratio between the quiescent output current and its maximum allowable value.

As a consequence, the classification reported in Table 1.2 and graphically depicted in Fig. 1.23 results.

Note that the definition based on the CCA is misleading, since the latter quantity is in fact a function of the device input drive. If a Class C (AB) PA is considered, an increase in input drive level typically results in an increase (decrease) of the CCA. The same effect does not hold for Class A or B PAs, at least to a first approximation. Obviously, if the drive level is further increased up to high compression regions (i.e. the amplifiers are *overdriven* or *saturated*), even in these cases a CCA variation occurs.

24 HIGH EFFICIENCY SOLID STATE POWER AMPLIFIERS

Table 1.2 Classification of PAs in term of output current conduction angle Φ or biasing point.

Operating Class	Current Conduction Angle CCA (Φ)	Dependence on Drive Level	Bias
A	$\Phi = 2\pi$	No	<i>Midway between Device Pinch-off and Saturation regions</i>
AB	$\pi < \Phi < 2\pi$	<i>Yes</i>	<i>Above Pinch-off</i>
B	$\Phi = \pi$	<i>No</i>	<i>Device Pinch-off</i>
C	$\Phi < \pi$	<i>Yes</i>	<i>Below Pinch-off</i>

On the contrary, the classification based on the bias point is typically adopted regardless of the PA drive level, in order to simply indicate the biasing region of the active device as determined by its quiescent supply conditions.

In this book the nomenclature Class A, AB, B or C will therefore be adopted according to the second definition (i.e. quiescent bias point selection).

In the biasing class grouping, it is intrinsically assumed that the driving signal is a sinusoidal waveform and the active device behaves as a current source. Otherwise, if the active device acts as a switch, the previous classification loses its validity.

A second and more advanced amplifier classification is related to the active device dynamic operating conditions and consequently to the matching network terminating conditions.

In this case, basically two wide categories are identified, namely *current-mode* and *switching-mode* PAs. In the former it is assumed that the active device acts as a current source, voltage controlled (in the case of field-effect devices) or current controlled (bipolar junction devices). On the contrary, in the latter family it is assumed that the active device behaves as a switch (as ideal as possible): the resulting amplifier could be more properly considered as a DC-to-RF power converter rather than an amplifier, since the input-output transfer characteristics are marginally considered.

A detailed classification is further performed for both families. As will be discussed in detail in the following chapters, for current-mode amplifiers the classification is based on the harmonic terminations synthesized across the active device, i.e. on the wave-shaping criteria adopted with the aim to maximize

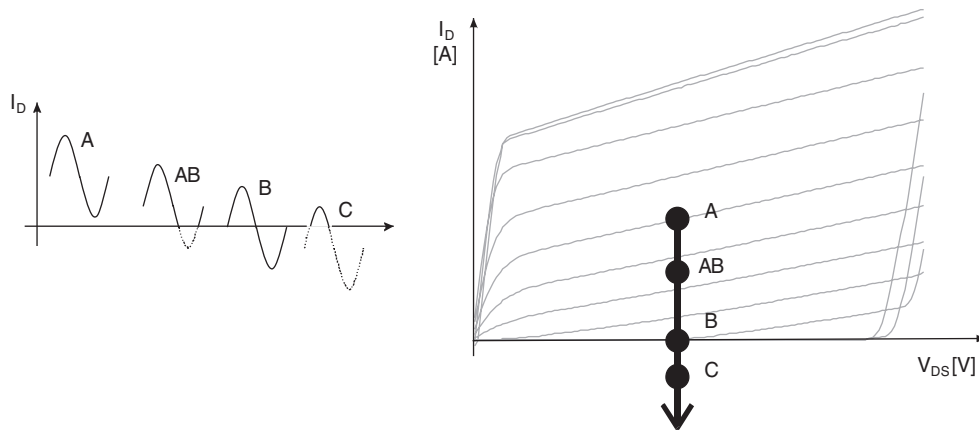


Figure 1.23 Class of operation defined as output current conduction angle (left) or simply by the device quiescent bias point (right).

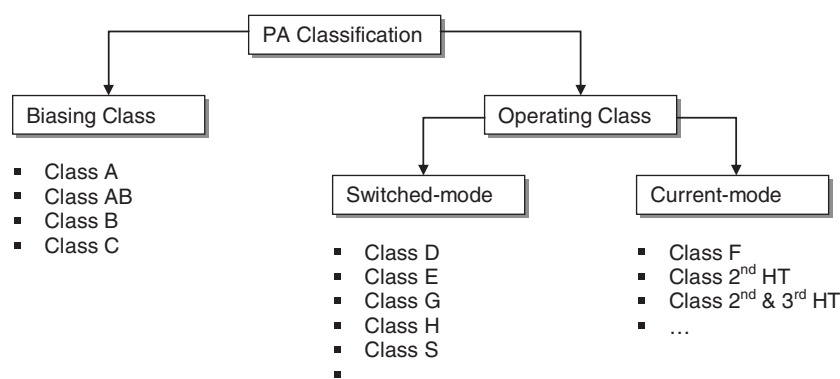


Figure 1.24 Structure of the PA classification.

output power, or efficiency or both. Examples of these classes are the Tuned Load, the Class F, the Harmonic Tuned and others.

Similarly, for the switched-mode amplifiers, a further classification is performed by identifying the switching duty-cycle and/or the switching combination, as for instance in Class E, Class D or Class S.

The PA classification structure just discussed is graphically summarized in Fig. 1.24.

In order to understand the power generating mechanisms in an active device and to infer design guidelines for each peculiar application, the two aspects of bias point selection and harmonic load conditions will be distinguished in the following chapters. In particular, an estimate of preliminary amplifier performance and the resulting dependence with the bias point selection will be inferred from simplified device modelling. Then the classes of operations referred to the operating conditions (current- or switching-mode) will be dealt with attempting a unifying approach, to identify the underlying criteria.

When an extremely linear PA is required, few guidelines are available to act directly during the design phase, being mainly inferred using Volterra analysis performed on the active devices. On the contrary, many more techniques are available for the distortion compensation (linearization) by means of external arrangements (predistortion, feedback, feedforward and other techniques). Therefore this case will be dealt with separately in chapter 9.

1.6 Overview of Semiconductors for PAs

The large differences in system applications where PAs are involved are necessarily reflected back into the active device technologies adopted for the PA module realization.

The early days of the microwave era were characterized by a massive use of vacuum tube devices [31–34], both for microwave signal generation and amplification. If microwave electronics may be dated back to the pioneering work of H. Hertz and J. C. Bose [35–38], a major push towards high power microwave generation and use came from the Second World War military applications in the radar field, with the introduction and use of the cavity magnetron by British researchers and the klystron as high power source in 1939–1940. The klystron evolved in Stanford University towards a high average power amplifier, leading to even modern applications involving clustered cavity klystron and travelling-wave tube [39–41].

In this scenario, solid state devices and the related amplifiers are relatively recent players, being the first GaAs MESFET, with good performance at X-band, commercially available at the beginning of the 1970s, despite the introduction of the device in the early work of Stuetzer and Shockley [42, 43].

26 HIGH EFFICIENCY SOLID STATE POWER AMPLIFIERS

Technology rapidly advanced and, in the 1970s, the development of techniques for semiconductor crystal growth such as molecular-beam epitaxy (MBE) allowed optimized p-n junction structures to be realized: a series of two- and three-terminal devices fabricated with frequency operation ranging from a few GHz well into the millimetre-wave region emerged [44–46]. IMPATT transit time and Gunn transferred electron devices can be assigned to the two-terminal device category. They have been and are still used both for frequency generation and amplification, as negative resistance amplifier, in the millimetre-wave region.

The broader and much more frequently used category of three-terminal devices comprises the already mentioned metal-semiconductor field-effect device (MESFET), the high electron mobility transistor (HEMT, demonstrated by Mimura in 1980 [44]) with its pseudomorphic (PHEMT) and metamorphic (MHMT) variants, the heterojunction bipolar transistor (HBT, introduced by Kroemer in 1957 [47]), and finally, due to the recent major advances of high frequency silicon technology, MOS and bipolar silicon transistors. Nevertheless, the ‘working horse’ technology for microwave power amplification is indeed based on III-V technologies, mainly of the GaAs material system. The latter technology is capable of providing, as the output of a single device, output power levels in the order of 100 W [48, 49] with operating frequencies approaching W-band. In the upper frequency range, InP solutions are more appropriate, even if providing very limited output power levels.

Even if ‘combined device’ concepts utilizing both solid-state and vacuum tube devices have been proposed, the former are generally utilized for low to moderate power output, while the latter is indeed necessary whenever high power and high operating frequency are targeted, as schematically indicated in Fig. 1.25 [50].

Output power performance of the given device type follows approximately a well-known behaviour if considered in its limit frequency region, i.e. the $P \cdot f^2 = const$ law:

$$P \cdot f^2 = const \tag{1.61}$$

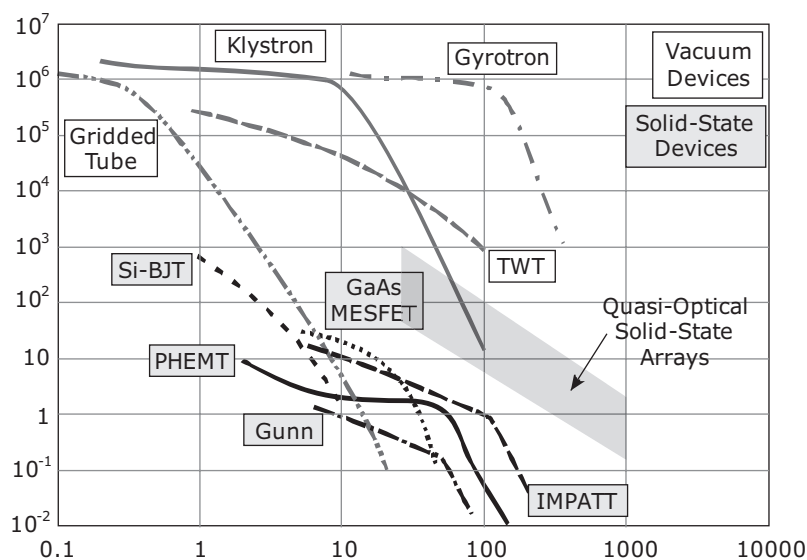


Figure 1.25 Single device output power as a function of frequency for solid-state and vacuum devices [50].

If a higher power is needed, solid state device outputs can be combined utilizing a series of different techniques, resulting in solid-state power amplifiers with output powers comparable to those of a vacuum tube source (i.e. in the kW region) in the microwave frequency region (up to X-band). On the other hand, as operating frequency increases, practical limitations arise from the systematic application of combining techniques, thus imposing the use of vacuum devices.

The recent trends towards higher and higher power densities, mainly pushed by radar and electronic warfare applications, is the latest development of the growth experienced by the high-frequency semiconductor industry. The increase in solid-state single-device performance is demanded for new device concepts and developing technologies. Among the latter ones, SiC [51] and GaN wide-bandgap semiconductor technologies are actually being explored: while SiC MESFET and HEMT have demonstrated 4–5 W/mm output power all through the X-band [52], nitride-based components are extremely promising, setting new upper limits to device performance in the range over 30 W per millimetre of device periphery, as compared to the 1–2 W limit of GaAs FET-based technologies and to the 2–4 W of the HBT ones [53–55]. Even if experimentally demonstrated in the microwave range, such performance is being exported to higher operating frequencies, well into the millimetre-wave spectrum.

Moreover, in the last decade, mobile and personal communications systems, ranging from cellular telephony to wireless LAN, with the corresponding request of high quality radio links, is posing a major challenge to high frequency technologies and subsystem performance, above all in the microwave frequency region.

In such a scenario, where many device technologies are potential candidates for a given application, above all in the low microwave region, the choice is indeed still open. As an example, in base station power amplifiers two main technologies are widely used: silicon LDMOS and GaAs. Both technologies can deliver output powers over 100 W in the L-band. But new device technologies like SiC and mainly GaN have to compete against these established ones. For other applications, as in wireless handsets, variants of HBT device technology are sometimes used.

The demand for portable apparatus, whose main characteristic is battery duration and overall size, translates naturally into a low-power electronic system. Since the PA in the transmitter section represents clearly the main source of supply power consumption, such a feature is directly transferred to its specifications. The PA designer is therefore faced with a difficult trade-off among the contrasting goals of high transmitted power, low power consumption and, for many telecom systems, linear operation. Given the widespread diffusion of many telecom applications, all of the above specifications have to be fulfilled keeping unit cost to a minimum. The resulting compromise may vary depending on the type of radio link to be established and overall system specifications, but their challenge has heavily influenced industrial, technical and research directions of the last decade in the PA field.

As a consequence, the high frequency semiconductor industry finally moved towards high volume production, implying processing 4- and 6-inch substrates with a corresponding increase in reproducibility, wafer uniformity and lower costs. Such a move had many beneficial effects on PA performance in terms of process maturity and stage performance. From the device side, GaAs FET discrete packaged power devices are actually produced and commercialized allowing high output power (up to 40 W in S-band in partially matched conditions or up to over 100 W directly in push-pull configuration for base station applications) even in X- or Ku-band (over 20 W in internally matched configuration in 14–14.5 GHz range).

In particular, the search for high output power is pushing, from the technological point of view, towards the design of active devices with high power densities, simultaneously exhibiting high reliability, reproducibility and at a very low cost. Six-inch wafers are currently adopted for high volume production in GaAs, as compared with the former prototyping 3- or 4-inch productions. Where the inherent difficulties of material growth and resulting quality are encountered, metamorphic solutions have been proposed, allowing the growth of high quality materials on a solid and reliable bulk substrate: this is the case of InP devices and structures utilizing GaAs wafers. The inherent volume and cost advantage is

28 HIGH EFFICIENCY SOLID STATE POWER AMPLIFIERS

evident, with minor performance degradation: the latter is mainly due to quality of the transition between materials, gradually accommodating the lattice mismatch, which can be appropriately optimized.

Due to the extremely diversified fields, figure of merits (FOMs) are used to characterize the devices adopted in PA design and realization. For high power applications important FOMs are indeed the device cut-off frequency f_T , the maximum oscillation frequency f_{Max} and obviously the RF output power P_{out} . Since P_{out} depends on the maximum voltage and current swings as previously underlined, other important FOMs for high power applications are the breakdown voltage V_{BR} and the maximum current per unit width of the device.

Equally important, especially for wireless application, is the device efficiency, which will be reflected in the amplifier conversion efficiency, relating the DC supply power to the actual delivered output power.

Other relevant aspects are related to device parasitic capacitances, which play an important role in circuit design. In fact, since high power devices offer a high transconductance, feedback capacitances, such as the gate-drain or base-collector ones, should be as low as possible to guarantee device stability. Moreover, power devices usually have to be matched to an optimum load to extract the highest possible output power. This optimum termination could be a very low impedance one, due to the device output capacitance, resulting in a difficult output matching network design, especially in broadband applications.

1.7 Devices for PA

Solid state active device performance relies upon the properties of semiconductor materials from which the devices are fabricated, including mechanical, electrical and thermal features [56]. For power applications, the main figures are represented by the power compression levels attainable from the single device, its power-added efficiency (thus implicitly accounting for the power gain also) and the linearity performance (i.e. third-order intermodulation, AM/PM, etc.). Such figures have to be evidently related also to their operating frequencies. In RF and microwave applications, solid state devices typically operate either at high power and low frequency, or at low power and high frequency, while the design and fabrication of devices able to operate at both high power and high frequency is still extremely challenging from the reliability point of view. The reason for such technological concern can be easily understood if we refer to the power gain G in an active device, defined as the ratio between the output power that the active device can provide (P_{out}), and the input power required to drive it (P_{in}):

$$G \triangleq \frac{P_{out}}{P_{in}} = \left(\frac{I_{out}}{I_{in}} \right)^2 \cdot \frac{\text{Re}\{Z_{out}\}}{\text{Re}\{Z_{in}\}} \quad (1.62)$$

I_{out} being the output current provided from the device to an external load Z_{out} , while I_{in} is the input current flowing into the device, characterized by the equivalent input impedance Z_{in} .

The ratio between the output and input currents is referred to as the device current gain, defined as:

$$A_i \triangleq \frac{I_{out}}{I_{in}} \quad (1.63)$$

which typically shows a low-pass behaviour in frequency.

Consequently, the device power gain is simply represented by [13]:

$$G(f) \approx K \cdot \left(\frac{f_T}{f} \right)^2 \cdot \frac{\text{Re}\{Z_{out}(f)\}}{\text{Re}\{Z_{in}(f)\}} \quad (1.64)$$

where K is a constant and f_T is the *cut-off frequency* of the device, defined as the frequency for which the current gain A_i falls down to unity.

From (1.62), to increase device power performance it is mandatory to increase its capabilities to provide higher output currents, typically implemented by increasing the number (i.e. arraying) of emitter/gate fingers. However, if the device output power is increased, the power dissipated in the device itself becomes proportionally augmented, resulting in non-uniform heat dissipation across the device fingers, leading to hotspots eventually causing device failure [57].

Moreover, long fingers imply in turn an increase of parasitic effects, thus reducing the cut-off frequency f_T . To avoid such issues, higher doping profiles could be adopted trying to preserve the output current I_{out} level. Nevertheless, a smaller breakdown voltage and thus reduced power capabilities result [58], if the device geometry and technology are not properly optimized (for instance using field-plate arrangements).

Continuing research activities result in the development of a variety of RF solid state devices, which can be roughly grouped into two main classes, i.e. the Bipolar-Junction Transistors (BJTs) or the Field Effect Transistors (FETs) [59, 60].

Among them, different and improved structures have been proposed, including Heterojunction Bipolar Transistors (HBTs) Metal Oxide Semiconductor Field Effect Transistors (MOSFETs), Laterally Diffused Metal Oxide Semiconductor FETs (LDMOSFET), Metal Semiconductor FETs (MESFETs) and High Electron Mobility Transistors (HEMTs), as schematically depicted in Fig. 1.26.

1.7.1 Requirements for Power Devices

The realization of high power devices requires an appropriate selection of semiconductor materials and a suitable placing of the emitter/gate fingers to properly balance the heat transfer across the device itself and to avoid peaking junction temperature, thus preventing device failures [59, 60].

Large-scale RF and microwave power device production, especially for commercial purposes, is actually based on silicon (Si), gallium arsenide (GaAs) and related compounds, while great research interest is devoted in the development of high power density devices using wide-bandgap materials such as silicon carbide (SiC) and gallium nitride (GaN).

The main substrate properties affecting the device performance, reported in Table 1.3, are represented by the material energy bandgap, the breakdown field, the thermal conductivity, electrons and holes transport properties, the saturated electron velocity and the conductivity which affects the loss behaviour at RF frequencies.

The energy bandgap, defined as the energy required for transferring an electron from the valence to conduction bands in a semiconductor, affects both the maximum allowed temperature in the device and

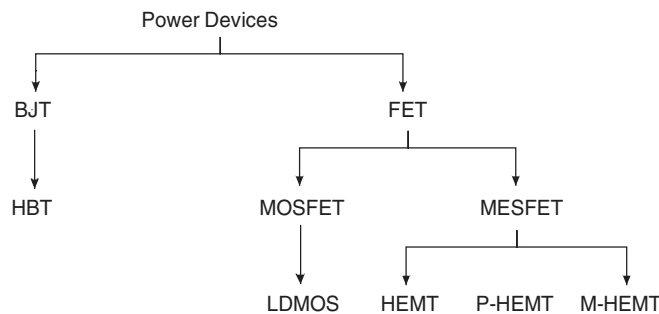


Figure 1.26 RF power device family tree.

30 HIGH EFFICIENCY SOLID STATE POWER AMPLIFIERS

Table 1.3 Semiconductor properties.

Property	Si	Ge	GaAs	GaN	4H-SiC	InP
Electron mobility ($\text{cm}^2 \text{V}^{-1} \cdot \text{s}^{-1}$)	1500	3900	8500	1000	900	5400
Hole mobility ($\text{cm}^2 \text{V}^{-1} \cdot \text{s}^{-1}$)	450	1900	400	350	120	200
Bandgap (eV)	1.12	0.66	1.42	3.2	3.23	1.35
Avalanche field (10^5 V/cm)	3.8	2.3	4.2	50	35	5.0
Saturated drift velocity (10^7 cm/s)	0.7	0.6	2.0	1.8	0.8	2.0
Saturation field (10^3 V/cm)	8		3	15	25	25
Thermal conductivity at 25°C ($\text{W/cm}\cdot^\circ\text{C}$)	1.4	0.6	0.45	1.7	4.9	0.68
Dielectric constant	11.9		12.9	14	10	8
Substrate resistance ($\Omega \text{ cm}$)			>1000	>1000	1–20	>1000
Transistors			MESFET			MESFET
			HEMT	MESFET	MESFET	HEMT
			HBT	HEMT	HEMT	HBT
			P-HEMT			P-HEMT

its power capabilities. A wider bandgap implies higher operating temperature [60] and smaller device sizes with increased power density (thus cheaper packaging requirements). Moreover, the large bandgap value leads to higher immunity to external influences (mandatory in a series of critical applications) and to the capability of supporting higher internal electric fields before the electronic breakdown event [60]. For these peculiarities, wide bandgap materials like GaN and SiC have been recently focused on and enormous research is going on to bring these material system to maturity and hence to the open market for the next generation of wireless and defence systems [61, 62].

The bandgap energy diagram for the main semiconductors is indicated in Fig. 1.27 as a function of the lattice constant. The latter becomes the key factor in compound semiconductor systems, in order to avoid strains and prevent detrimental trapping phenomena.

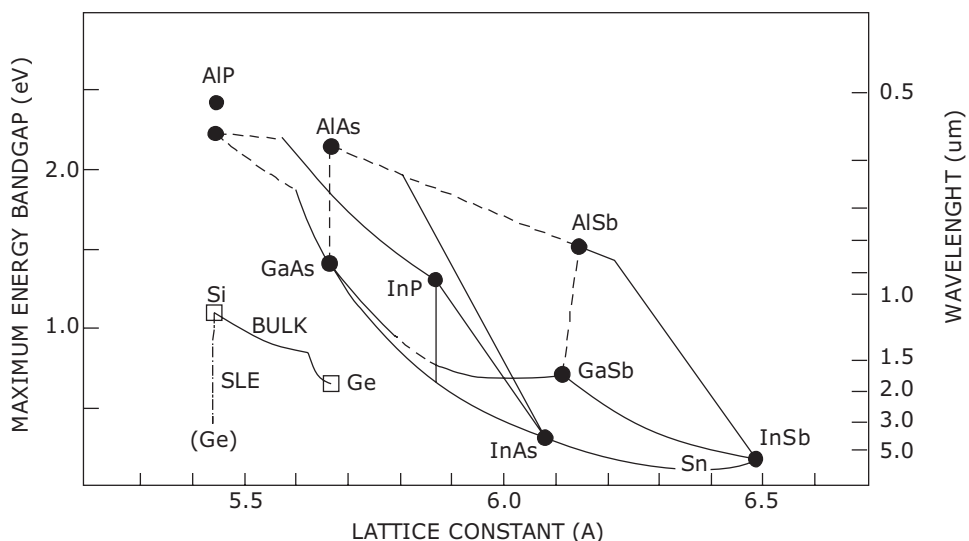


Figure 1.27 Bandgap energy and wavelength vs. lattice constant.

As seen in Table 1.3, a higher bandgap corresponds to a higher breakdown field, which in turns implies the capability of the device to allow higher output voltage swings and thus to attain higher output power levels.

Moreover, the high breakdown voltage results in larger output impedance values for a given current density, making device matching easier during the circuit synthesis. Similarly, the dielectric constant is an indication of the capacitive loading of a device, thus a low value is generally desired.

Nevertheless, increasing the power density in actual devices, the heat disposal becomes a major issue: the thermal conductivity of the adopted material system becomes critical, to avoid the power dissipated in the active device increasing the junction temperature and degrading the device performance and reliability.

Regarding the substrate resistance, this figure becomes critical in laterally developed devices, since an insulating substrate decreases losses at microwave frequencies.

Finally, electron and hole mobilities mainly determine the electrically ON resistance and knee voltage of a power device. A low mobility results in increased parasitic resistance, increased losses and reduced gain, thus clearly limiting the frequency of operation.

1.7.2 BJT

The BJT is one of the most essential semiconductor devices, mainly fabricated over silicon in a vertical structure, as schematically depicted in Fig. 1.28.

The structure is formed by diffusing a p-type region between a heavily doped n^+ region and a n-type substrate. The heavily doped n^+ region is called the emitter (E), the centre of the p region is called the base (B) and the lightly doped n region is the collector (C) [59].

Since RF power BJTs are usually realized by composing multiple small BJTs, emitter ballasting is generally employed to force even division of the current within a given package [63]. The Si BJT typically operates from 28 V of bias supply and is adopted up to 5 GHz especially in high power (1 kW) pulsed applications (e.g. radar [64]).

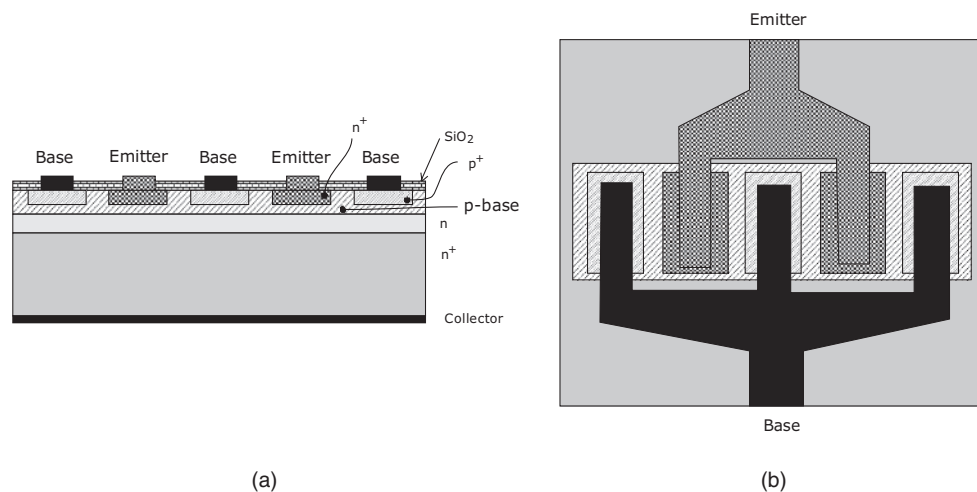


Figure 1.28 Schematic structure of a BJT (a) and its top view (b).

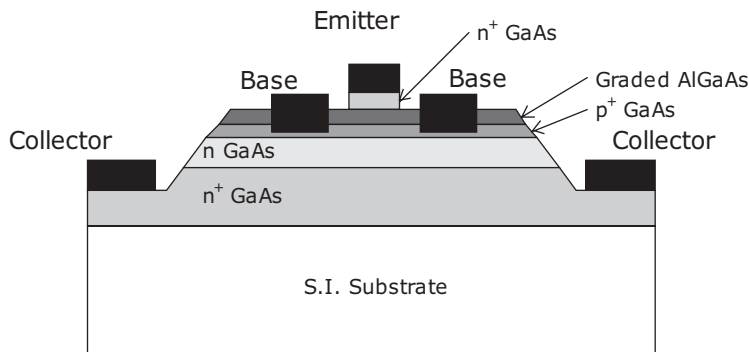


Figure 1.29 Schematic structure of a HBT.

1.7.3 HBT

The HBTs represent the natural improvement of conventional BJTs, as a result of the exploitation of heterostructure junctions [60]. Such heterostructures are typically based on compound semiconductor materials like AlGaAs/GaAs, SiGe and InP, as schematically depicted in Fig. 1.29 for a GaAs HBT.

In order to minimize the base resistance, the emitter is realized as narrow as possible, while the barrier is created directly by the heterojunction (AlGaAs/GaAs in Fig. 1.29) rather than by the doping profile.

Unlike conventional BJTs, in HBTs the bandgap difference between the emitter and the base materials results in higher common emitter gain. Base sheet resistance is lower than in ordinary BJTs, and the resulting operating frequency is accordingly higher [59]. The current flow path is vertical, so that surface imperfections affect marginally the device performance. Furthermore, the use of a semi-insulating substrate and the higher electron mobility result in reduced parasitics.

GaAs HBT are widely used in MMICs and they operate in PAs at frequencies as high as 20 GHz, while with InP HBT operation up to 50 or 60 GHz has been demonstrated [64].

Recently, the lately arrived Si/SiGe HBT is rapidly invading the RF and wireless systems market, due to its strong affinity with more conventional silicon bipolar devices, thus simplifying the conversion to the new technology in many cases. Nowadays Si/SiGe BiCMOS technologies are commercially available in a number of foundries ranging from 0.50 μm high-voltage to 0.18 μm high-speed technologies [65]. However, the power handling capability for a unit device is reduced, making the realization of a power amplifier in Si/SiGe BiCMOS suitable for millimetre-wave operation particularly challenging [66].

The main advantage of HBT with respect to FET devices, where PAs are concerned, is represented by the higher linearity of the former, which seems to be related to the base-emitter junction capacitance and its beneficial effect in reducing the intermodulation products [67].

1.7.4 FET

The FET family includes a variety of structures, among which are MESFETs, MOSFETs, HEMTS, LDMOS, etc.² They typically consist of a conductive channel accessed by two ohmic contacts, acting as a source (S) and as a drain (D) terminals respectively. The third terminal, the gate (G), forms a rectifying

²JFETs are other classes of FET devices for power applications, characterized by very large (impressive) power and efficiency for devices based upon Si, SiGe, and SiC up to UHF frequencies. The device has never become as popular as other RF-power FETs [64] due to its poor performance while the frequency is increased.

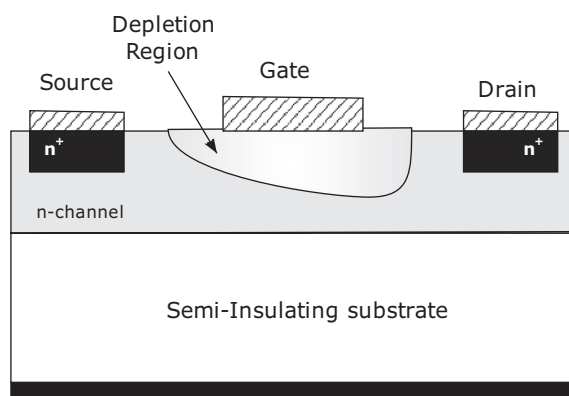


Figure 1.30 Simplified structure of FET [59].

junction with the channel or a MOS structure. A simplified structure of a metal-semiconductor n-type FET is depicted in Fig. 1.30.

Applying a positive voltage V_{ds} between drain and source terminals, electrons flow from the source to the drain, thus creating a current I_d in the channel beneath the gate. Thus the source acts as origin of carriers while the drain becomes the sink, and the current flux can be controlled by the rectifying junction formed by the gate terminal and the channel. The gate electrode is deposited to form a Schottky diode in a JFET or MESFET and a metal-oxide (insulator) system in a MOSFETs [59].

FET devices ideally do not draw current through the gate terminal, unlike the BJTs which conversely require a significant base current, thus simplifying the biasing arrangement.

Moreover, FET devices exhibit a negative temperature coefficient, resulting in a decreasing drain current as the temperature increases. This prevents thermal runaway and allows multiple FETs to be connected in parallel without ballasting, a useful property if a corporate or combined device concept has to be adopted for high power amplifier design.

The device performance is critically determined, over the material properties, by geometrical parameters like the length, width, depth of the channel and depletion layer width [59].

In general, the length of the channel under the gate determines the transit time, i.e. the time required by electrons to travel through the channel itself. This transit time determines the cut-off frequency f_T and the maximum frequency f_{Max} . At the same time, however, channel length and inter-electrode spacing (eventually with field-plate arrangements) influence the maximum operating voltage of the transistor, being also determined by the breakdown field of the material.

1.7.5 MOSFET

These devices are realized by growing an insulated gate above the channel. The latter, according to the doping profile selected, could be already formed (depletion device) or must be created (enhancement device) by suitable gate voltages. As an example, a typical enhancement structure is depicted in Fig. 1.31 [60], but topologies with both vertical and lateral current flow are used in RF applications, most of them produced by a double-diffusion process [68].

The standard material used as substrate to grow MOSFET is silicon, whose technology process is sufficiently mature, allowing also the realization of stable oxide used as the dielectric to realize the oxide insulator beneath the gate.

34 HIGH EFFICIENCY SOLID STATE POWER AMPLIFIERS

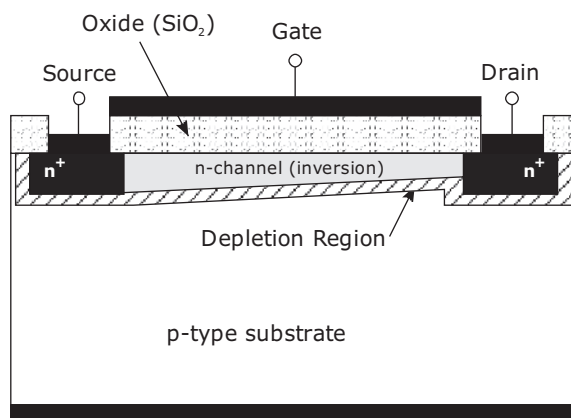


Figure 1.31 Enhanced n-MOSFET device cross-section.

The main issues of MOSFET device are intrinsically related to the oxide insulator, and in particular to the presence of unavoidable traps, which imply a shift in the voltage threshold, and in the unavoidable parasitics connected with the MOS structure (capacitive in nature) reducing the maximum operating frequency.

1.7.6 LDMOS

LDMOS is an enhanced MOSFET structure especially suited for high power applications. Its basic structure is schematically indicated in Fig. 1.32 [69]. In a LDMOS, as in a MOSFET, there are two n^+ regions for the source and the drain respectively. The most noticeable difference as compared to a

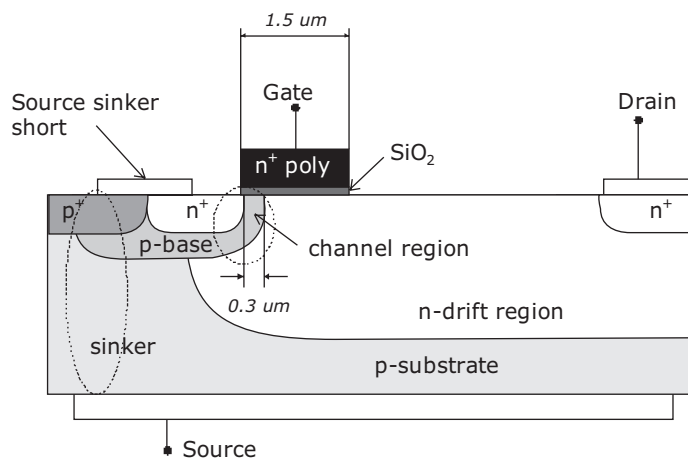


Figure 1.32 Cross-section of a LDMOS.

MOSFET is in the low doped and quite long n-drift region realized in the LDMOS, which enhances the depletion region.

Separating the channel region from the drift region allows designing a short channel device for high frequency operation. At the same time, the increased distance between the drain and source allows higher voltage operation without reaching the breakdown field of the device, thus resulting in higher power capabilities.

The LDMOS drain current follows the same behaviour as in a MOSFET. Applying a positive voltage to the gate, a conductive channel in the p-base region is created. The channel being very short, the device transistor always operates in the saturated velocity region, thus further improving device linearity [70, 71]. Electrons with saturation velocity at the channel flow in the doped n-drift region reaching the drain.

The LDMOS is especially useful at UHF and lower microwave frequencies, since the direct grounding of its source eliminates bond-wire inductance that produces negative feedback and reduces gain at high frequencies. Currently, packaged LDMOS devices typically operating from 28 V supplies and they are available with output powers over 120 W at 2 GHz.

1.7.7 MESFET

MESFETs have a structure and DC characteristics quite similar to MOSFETs, but differing from the latter since in a MESFET the gate electrode uses a metal semiconductor contact instead of a MOS arrangement. A typical structure of a MESFET is depicted in Fig. 1.33. There are two n^+ regions, one for source and the other for the drain, while an n-type channel is present between drain and source terminals and connected to the gate by a Schottky junction. This implies that normally a MESFET device is active for $V_{GS} = 0$ V, thus operating in a depletion-mode requiring negative gate bias, although also enhancement-mode devices that operate with a positive bias have been developed [72].

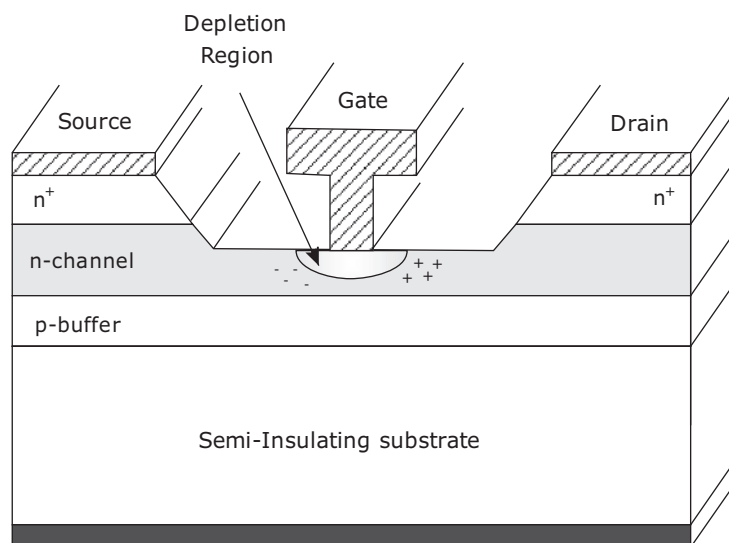


Figure 1.33 MESFET device cross-section.

36 HIGH EFFICIENCY SOLID STATE POWER AMPLIFIERS

The source is usually grounded (common source configuration) and the drain is positively biased. Applying a negative gate source voltage reverse biases the metal semiconductor junction, thus forming a depletion layer in the channel. An increase in the negative gate voltage causes an increase in the depletion region, and a decrease in the conductive channel width: control of the current flow between the drain and source is thus achieved.

MESFET devices are usually fabricated from III-V compound semiconductors; the predominant is GaAs, or more recently from wide-bandgap semiconductors like SiC [64].

Since III-V compound semiconductors do not allow stable oxide to make the gate dielectric, a Schottky metal semiconductor contact is instead used for the gate. The adoption of Schottky gate results in two main advantages: to avoid traps in the gate insulator, affecting the threshold voltage shift in the MOSFETs [60], and the absence of the capacitor formed from the channel (conductor), dielectric (insulator) and metal gate terminal (conductor) in normal MOSFET structure, thus allowing higher frequency operation.

Moreover, MESFET based on a GaAs (or SiC) substrate and a Schottky gate junction, exhibit a higher mobility than Si MOSFET devices, thus making them capable of operating with acceptable gain and efficiently at higher frequencies.

The SiC devices, due to their wide energy bandgap and the higher thermal conductivity, provide higher power densities, up to 10 W/mm, with respect to the typical values 0.3–0.5 W/mm of GaAs based MESFETs.

SiC MESFETs typically operate from 50 to 60 V of DC voltage supply [73], with some demonstrations extending to hundreds of volts, while GaAs MESFETs are typically operated from supply voltages (drain biases) of 5–10 V [64].

The higher operating voltage and associated higher load impedance of SiC greatly simplify output networks and power combining. However, the lower carrier mobility in SiC, together with a lower transconductance value (typically 120 mS/mm as compared as to 159 mS/mm of GaAs device), reduces the frequency range of such devices up to 10–12 GHz maximum, against the 25–30 GHz of GaAs MESFETs [74].

GaAs MESFETs, however, are widely used for the production of microwave power, with capabilities of over hundreds of watts in the L-band or tens of watts up to K-band for packaged devices.

As previously outlined, the negative temperature coefficient, which prevents thermal runaway, allows multiple MESFETs to be easily connected in parallel, thus realizing a larger device, as for instance reported in Fig. 1.34 [75].

In terms of linearity, MESFET devices exhibit a slightly worse performance as compared to HBTs, due to both the input (gate-channel junction) and the output (drain-channel-source) capacitive parasitics which are often strongly bias and frequency dependent.

The cost of SiC devices is currently about ten times that of a Si LDMOS, which clearly, up to now, is the ultimate affordable choice for use in high power transmitters and base stations operated at 900 MHz and 2 GHz [64].

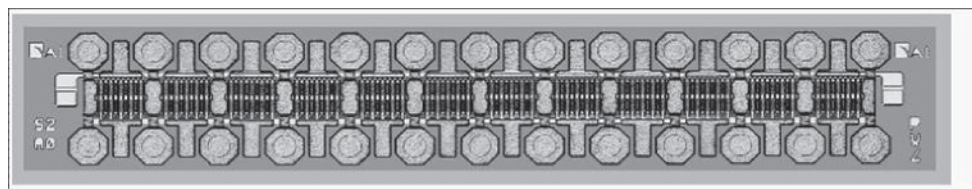


Figure 1.34 Picture of a 6W GaAs MESFET (3×0.6mm) at X-band (courtesy of Selex-SI).

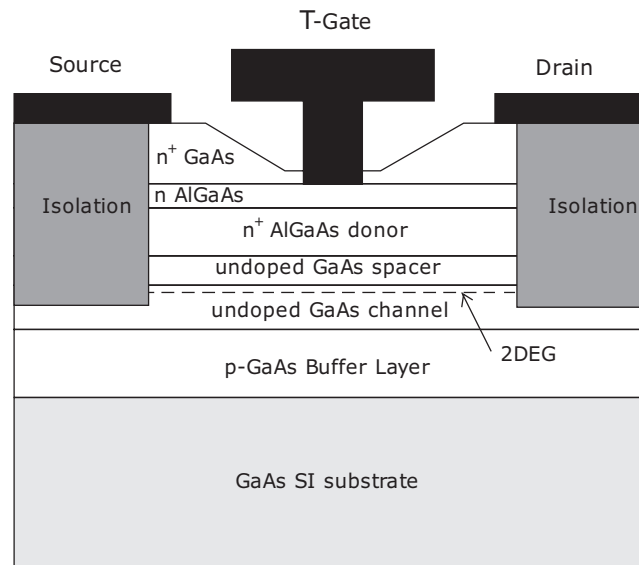


Figure 1.35 Structure of a AlGaAs/GaAs HEMT.

1.7.8 HEMT

In HEMT's devices the conducting layers are epitaxially grown over a semi-insulating substrate realizing a heterostructure alongside the electron flow, as schematically depicted in Fig. 1.35 for a AlGaAs/GaAs HEMT.

The typical materials used for HEMT's are AlGaAs, Al/InGaAs and AlGaN [60].

The heterojunction formed (e.g. by AlGaAs/GaAs in Fig. 1.35) results in a sharp dip in the conduction band edge, as schematically reported in Fig. 1.36, forming a potential well.

Such a discontinuity in the bandgaps of AlGaAs and GaAs causes a thin layer of electrons, i.e. a high carrier concentration in a confined region below the gate at the interface of the AlGaAs and GaAs layers, forming the so-called two-dimensional electron gas (2-DEG).

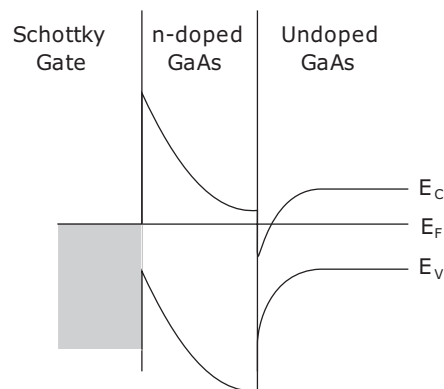


Figure 1.36 Band diagram of a AlGaAs/GaAs HEMT.

38 HIGH EFFICIENCY SOLID STATE POWER AMPLIFIERS

Since the 2-DEG is created in an undoped GaAs layer, the carriers in this 2-DEG do not suffer from scattering by ionized donor atoms, thus resulting in reduced collision phenomena as compared to classical MESFET, and hence in a higher frequency response, typically increased by a factor of 2, justifying the preference of HEMT instead of MESFET for microwave applications [58].

The structure of the InP HEMT is quite similar to AlGaAs/GaAs one, except that an AlInAs/GaInAs heterojunction on an InP substrate is used. In this case the material lattice constants are more closely matched, thus allowing a large amount of In content, which in turns implies an increased carrier mobility, an increased 2-DEG and a higher transconductance, thus resulting in higher frequency operations [60]. However, the lower thermal resistance of InP as compared as to GaAs substrate, with the lower breakdown voltage, results in a reduced power handling capability of the InP HEMT. Nonetheless, InP HEMTs have been fabricated with f_{Max} as high as 600 GHz (0.1 μm gate lengths and lower, down to 35 nm), and amplification has been demonstrated at frequencies as high as 300 GHz, while typical power range from 100 to 500 mW per chip have been demonstrated [64].

In GaN HEMTs, the heterostructure is formed using AlGaN/GaN. Since GaN devices are realized on different semiconductors (silicon) or semiconductor alloys (SiC), the thermal conductivity of the overall device is strongly dependent on the adopted substrate.

Since substrate material growth is to date particularly cumbersome (with some exceptions), for high power applications a SiC substrate is used, over which the GaN epitaxy is grown, layer by layer. The thermal conduction properties of the GaN HEMT are therefore the good properties of the SiC substrate. While the GaN HEMT offers the promise of a high-power, high-voltage device operating at frequencies of 10 GHz or more, its technology it is still maturing, even if at an unprecedented speed.

For power transistors, in order to increase the charge density of the 2-DEG, multiple quantum wells are usually realized, as for instance depicted in Fig. 1.37 [76].

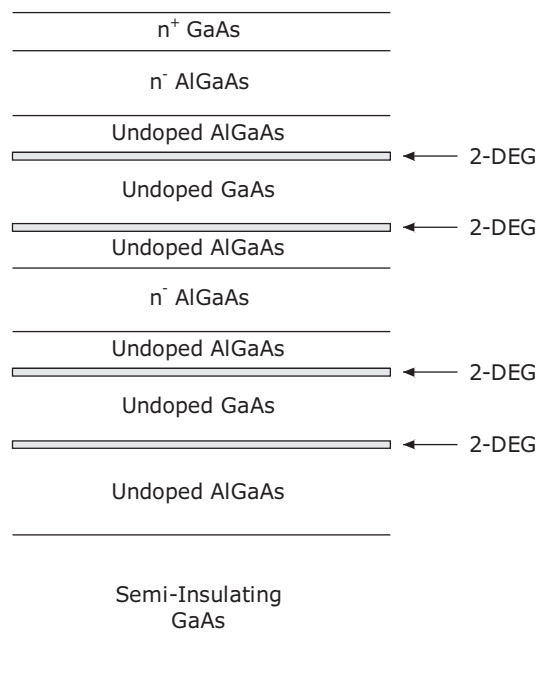


Figure 1.37 Multiple quantum well HEMT structure.

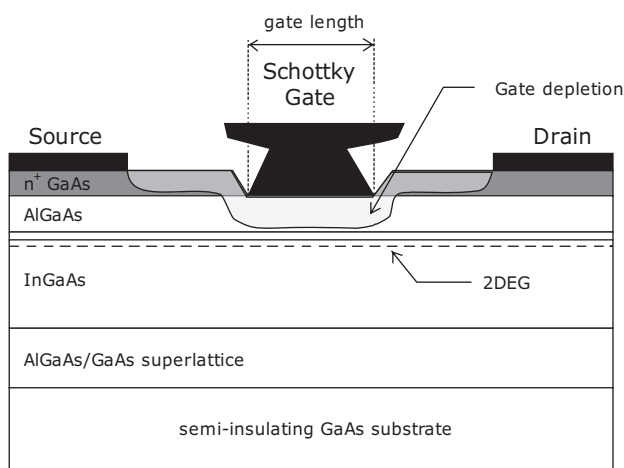


Figure 1.38 Structure of P-HEMT.

Moreover, to avoid scattering phenomena occurring between the electrons in the 2-DEG and ionized donors, an undoped AlGaAs layer (namely *spacer layer*) is inserted between the n-type AlGaAs and the undoped GaAs [60].

The pseudomorphic HEMT (P-HEMT) is a further improvement of classical HEMT structures, in which a material having a different lattice constant is used, thus creating a lattice mismatch. For instance, an InGaAs layer is used between the n AlGaAs spacer and the GaAs layer, as depicted in Fig. 1.38.

The resulting larger bandgap discontinuity creates more charge in the 2-DEG, thus increasing the transconductance and the output power [58].

The increased performance in terms of frequency and output power comes at the expense of a lattice mismatch between the layers. The mismatch results largely in the thin and compressed InGaAs layer, which is usually referred to as the pseudomorphic layer [76].

The mismatch is much more emphasized depending on the indium fraction in the layers. In order to ensure a device reliability, the indium fraction is typically maintained lower than 22% if a GaAs substrate is used, while it can be increased up to 50% if an InP substrate is adopted [64].

For power transistors, the higher breakdown values allowed by GaAs as compared to InP imply a preference of GaAs P-HEMT rather than InP P-HEMT [77].

In order to reduce lattice mismatch, in the metamorphic HEMT (M-HEMT), a relaxing layer is inserted between the GaAs substrate and the InGaAs channel, to properly adapt the different lattice constants, resulting in the structure depicted in Fig. 1.39.

The M-HEMTs are widely adopted for low noise high frequency applications [78], being characterized by a maximum operating frequency f_{Max} exceeding hundreds of GHz for devices with gate length of 0.1 μm and below [79].

On the contrary, due to the lower power density, the M-HEMTs are rarely adopted for power applications, especially for frequencies lower than 40–50 GHz, where the performance achievable with other technologies is superior [80].

HEMTs are known in the literature by a wide variety of different names, including MODFET (Modulation-Doped FET), TEGFET (Two-dimensional Electron-Gas FET), and SDFET (Selectively Doped FET). Cut-off frequencies f_T as high as 200 GHz have been reported for a series of GaAs HEMT structures with different indium content in the channel. PAs based upon HEMTs exhibit output power levels in excess of tens of watts at X-band and above.

40 HIGH EFFICIENCY SOLID STATE POWER AMPLIFIERS

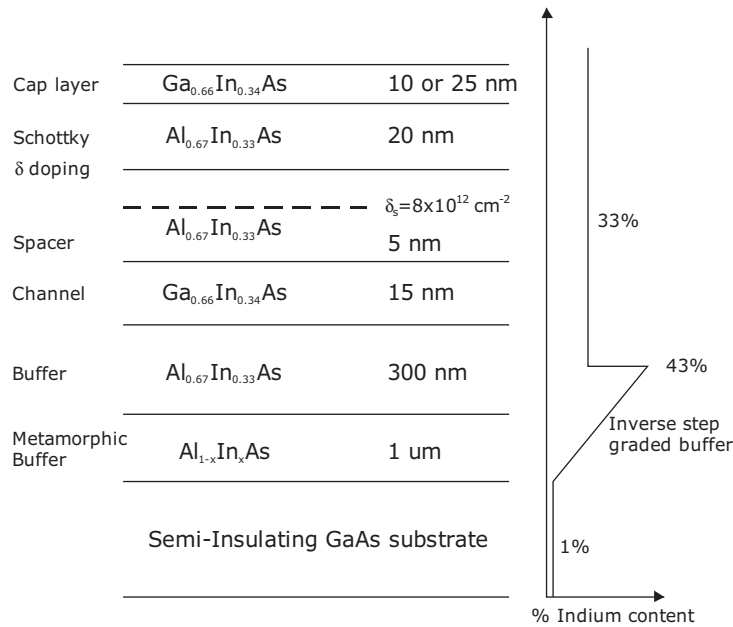


Figure 1.39 Structure of M-HEMT.

1.7.9 General Remarks

For power applications, the more mature and reliable technology is represented by devices in GaAs. However, this does not imply that it is also the best choice for all the operating frequencies. In fact, as previously outlined, in order to ensure the same current density, the device gate length and width have to be reduced increasing the operating frequency, while increasing the doping profile, thus inevitably resulting in a lower breakdown voltage and thus lower power density [81]. The MESFET devices are typically adopted for frequencies up to 18–20 GHz, while the adoption of heterojunction devices (mainly of the HEMT type) becomes mandatory for higher operating frequencies.

Similarly, in the low frequency range, say up to a few GHz, LDMOS devices have steadily carved the base station power market, at the expense of Si BJTs and GaAs MESFETs.

Recently, a great deal of attention has been given to SiGe HBTs, thanks to the capability of easy integration. However, the SiGe HBT device structure remains a relatively low power pattern, thus it is not a candidate for high power and high frequency applications.

Achievement of high power densities is a priority for RF power technologies as it reduces size, which is advantageous for both fixed and mobile platforms. Wide-bandgap devices such as SiC MESFETs and GaN HEMTs are of particular interest in this regard. RF output power densities of the order of 4–7 W/mm and 10–12 W/mm are achievable for SiC MESFETs and AlGaIn/GaN HEMTs respectively [82]. Achievement of high power density not only reduces size, it also provides higher working impedances, which are necessary for wider bandwidth operation, simpler circuits for RF matching and ease of manufacture.

SiC MESFETs benefit from the excellent thermal conductivity of its substrate. However, its electron mobility is significantly lower than that of GaN, which is related to the lack of availability of heterojunction technology in this material system.

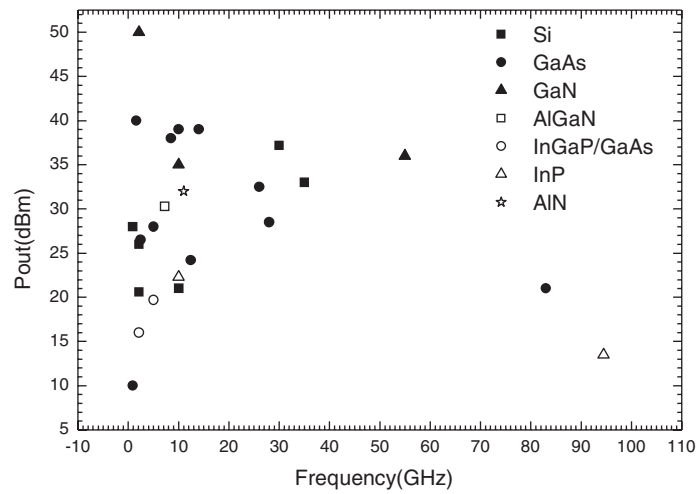


Figure 1.40 Output power vs. frequency for state-of-the-art high frequency active devices.

Further, the substrates are costly, limited in diameter and contain micro-pipe defects affecting device manufacture and yields. Unless the substrate problems are addressed in the near future, SiC MESFETs will have a difficult time competing in cost sensitive commercial applications such as base station power amplifiers for wireless communications systems.

As an example of achievable performance, Fig. 1.40 reports the output power levels achieved with PAs realized in solid state technology by using different material systems, while Fig. 1.41 evidences the efficiency levels attained.

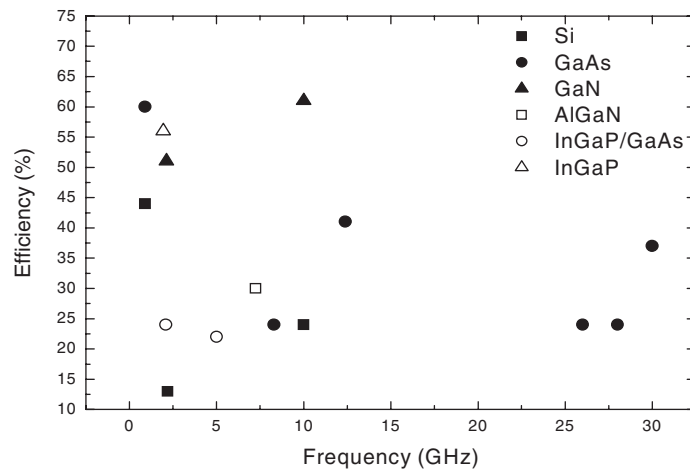


Figure 1.41 Efficiency vs. frequency for state-of-the-art high frequency active devices.

1.8 Appendix: Demonstration of Useful Relationships

In order to demonstrate expression (1.40), assuming the cubic amplifier model (1.22), if the input signal is a single tone with amplitude x_{1T} , then the output signal at fundamental frequency becomes (1.25):

$$y_{1T} = k_1 \cdot x_{1T} + \frac{3}{4}k_3 \cdot x_{1T}^3 \quad (1.65)$$

The input and output (fundamental) powers become respectively:

$$P_{in,1T}(f) = \frac{1}{2}x_{1T}^2 \quad (1.66)$$

$$P_{out,1T}(f) = \frac{1}{2}y_{1T}^2 \quad (1.67)$$

Thus at 1dB compression, the output power, related to the linear term only (K_1x), will be 1 dB higher than the power related to (1.67), i.e.

$$P_{out,1T,1dBc} = 10 \cdot \log_{10} \left[\frac{1}{2} (k_1 x_{1T,-1dB} + k_3 x_{1T,-1dB}^3)^2 \right] = 10 \cdot \log_{10} \left[\frac{1}{2} (k_1 x_{1T,-1dB})^2 \right] - 1 \quad (1.68)$$

Since

$$1 = 10 \cdot \log_{10}[10^{0.1}] \quad (1.69)$$

then

$$10 \cdot \log_{10} \left[\frac{1}{2} \left(k_1 x_{1T,-1dB} + \frac{3}{4} k_3 x_{1T,-1dB}^3 \right)^2 \right] = 10 \cdot \log_{10} \left[\frac{1}{2} \frac{(k_1 x_{1T,-1dB})^2}{10^{0.1}} \right] \quad (1.70)$$

from which, assuming that all terms in brackets are positive, it follows that

$$(1 - 10^{-0.05}) = -\frac{3}{4} \frac{k_3}{k_1} x_{1T,-1dB}^2 \quad (1.71)$$

If now a two-tone input signal is assumed, considering for both tones the amplitude x_{2T} , then the output power due to the linear term is (see Table 1.1)

$$P_{out,2T,linear}(f) = 10 \cdot \log_{10} \left[\frac{1}{2} (k_1 x_{2T})^2 \right] \quad (1.72)$$

while the output power of the third-order IMD product is given by:

$$P_{out,2T}(2f_2 - f_1) = 10 \cdot \log_{10} \left[\frac{1}{2} \left(\frac{3}{4} k_3 x_{2T}^3 \right)^2 \right] \quad (1.73)$$

Therefore, to infer the $IP3$, it is required to equate both power levels, i.e.

$$P_{out,2T,linear}(f) = P_{out,2T}(2f_2 - f_1) \quad (1.74)$$

from which

$$x_{2T,IP3}^2 = \left(\frac{3}{4} k_3 x_{2T,IP3}^3 \right)^2 \quad (1.75)$$

Assuming for k_3 a negative value (corresponding to a gain compression behaviour), it follows that

$$-\frac{3}{4} \frac{k_3}{k_1} x_{2T,IP3}^2 = 1 \quad (1.76)$$

Finally, comparing (1.71) and (1.76):

$$\left(\frac{x_{2T,IP3}}{x_{1T,-1dB}} \right)^2 = \frac{1}{1 - 10^{-0.05}} \approx 9.2 \quad (\approx 9.6dB) \quad (1.77)$$

Therefore, for the input power level it follows that:

$$IP3_{in} - P_{in,1T,-1dBc} \approx 9.6dB \quad (1.78)$$

Now, remembering that in a logarithmic scale

$$\begin{aligned} IP3_{out} &= IP3_{in} + G_L \\ P_{out,1T,-1dBc} &= P_{in,1T,-1dBc} + G_L - 1 \end{aligned} \quad (1.79)$$

then

$$IP3_{out} \approx P_{out,1T,-1dB} + 10.6 \text{ dB} \quad (1.80)$$

A similar procedure can be adopted to demonstrate (1.41). In particular, when two tones of equal amplitude are applied to the PA input, for the 1 dB compression point the following relation can be inferred (see Table 1.1)

$$\begin{aligned} P_{out,2T,-1dB} &= 10 \cdot \log_{10} \left[\frac{1}{2} \left(k_1 x_{2T,-1dB} + \frac{3}{4} k_3 x_{2T,-1dB}^3 + \frac{3}{2} k_3 x_{2T,-1dB}^3 \right)^2 \right] \\ &= 10 \cdot \log_{10} \left[\frac{1}{2} (k_1 x_{2T,-1dB})^2 \right] - 1 \end{aligned} \quad (1.81)$$

from which

$$(1 - 10^{-0.05}) = -\frac{k_3}{k_1} \frac{9}{4} x_{2T,-1dB}^2 \quad (1.82)$$

Thus, comparing (1.71) and (1.82) it follows that

$$\left(\frac{x_{2T,-1dB}}{x_{1T,-1dB}} \right)^2 = \frac{1}{3} \quad (\approx -4.77dB) \quad (1.83)$$

and

$$P_{out,2T,-1dB} \approx P_{out,1T,-1dB} - 4.77 \text{ dB} \quad (1.84)$$

44 HIGH EFFICIENCY SOLID STATE POWER AMPLIFIERS

Finally, to demonstrate relationship (1.42), simple geometrical observations are applied. In particular the point $IP3_{out}$ is obtained by the intersection of the extrapolation of the output power at the fundamental (linear behaviour, slope of 1dB per dB), with the third-order intermodulation product P_{IMD} (slope 3dB per dB). This means that the following relationships hold:

$$\begin{aligned} IP3_{out} &= P_{out,dBm} + k \\ IP3_{out} &= P_{IMD} + 3 \cdot k \end{aligned} \quad (1.85)$$

from which

$$P_{IMD} = 3 \cdot P_{out,dBm} - 2 \cdot IP3_{out} \quad (1.86)$$

Moreover, for the C/I it follows that

$$\begin{aligned} \left(\frac{C}{I}\right)_{dBc} &= P_{out,dBm} - P_{IMD} = \\ &= P_{out,dBm} - (3 \cdot P_{out,dBm} - 2 \cdot IP3_{out}) = \\ &= 2 \cdot (IP3_{out} - P_{out,dBm}) \end{aligned} \quad (1.87)$$

1.9 References

- [1] H. Sobol, K. Tomiyasu, 'Milestones of microwaves,' *IEEE Trans. Microwave Theory Techn.*, Vol. 50, N. 3, March 2002, pp. 594–611.
- [2] M. Skolnik, 'Role of radar in microwaves,' *IEEE Trans. Microwave Theory Techn.*, Vol. 50, N. 3, Mar. 2002, pp. 625–632.
- [3] W. Keydel, 'Perspectives and visions for future SAR systems,' *IEE Proc. Radar, Sonar Navigat.*, Vol. 150, N. 3, June 2003, pp. 97–103.
- [4] B.A. Kopp, M. Borkowski, G. Jerinic, 'Transmit/receive modules,' *IEEE Trans. Microwave Theory Techn.*, Vol. 50, N. 3, March 2002, pp. 827–834.
- [5] J.M. Osepchuk, 'Microwave power applications,' *IEEE Trans. Microwave Theory Techn.*, Vol. 50, N. 3, March 2002, pp. 975–985.
- [6] J.M. Osepchuk, 'A history of microwave heating applications,' *IEEE Trans. Microwave Theory Techn.*, Vol. 32, N. 9, Sep. 1984, pp. 1200–1224.
- [7] A. Rosen, M.A. Stuchly, A. Vander Vorst, 'Applications of RF/microwaves in medicine,' *IEEE Trans. Microwave Theory Techn.*, Vol. 50, N. 3, March 2002, pp. 963–974.
- [8] G.C. Giakos, M. Pastorino, F. Russo, S. Chowdhury, N. Shah, W. Davros, 'Noninvasive imaging for the new century,' *IEEE Instrument. Measur. Mag.*, Vol. 2, N. 2, June 1999, pp. 32–35 and 49.
- [9] E.C. Fear, X. Li, S.C. Hagness, M.A. Stuchly, 'Confocal microwave imaging for breast cancer detection: localization of tumors in three dimensions,' *IEEE Trans. Biomed. Engng.*, Vol. 49, N. 8, Aug. 2002, pp. 812–822.
- [10] I.T. Rekanos, A. Raisanen, 'Microwave imaging in the time domain of buried multiple scatterers by using an FDTD-based optimization technique,' *IEEE Trans. Magnetics*, Vol. 39, N. 3, May 2003, pp. 1381–1384.
- [11] L.Q. Huo, W. Zhong, T.T. Qing Zhang, J.A. Bryan, G.A. Ybarra, L.W. Nolte, W.T. Joines, 'Active microwave imaging. I. 2-D forward and inverse scattering methods,' *IEEE Trans. Microwave Theory Techn.*, Vol. 50, N. 1, Jan. 2002, pp. 123–133.
- [12] E.C. Fear, P.M. Meaney, M.A. Stuchly, 'Microwaves for breast cancer detection?,' *IEEE Potentials*, Vol. 22, N. 1, Feb.-March 2003, pp. 12–18.
- [13] S.C. Cripps, *RF Power Amplifiers for Wireless Communications*, Norwood, MA, Artech House, 1999.

- [14] F.H. Raab, P. Asbeck, S. Cripps, P.B. Kenington, Z.B. Popovic, N. Potheary, J.F. Sevic, N.O. Sokal, 'Power amplifiers and transmitters for RF and microwave,' *IEEE Trans. Microwave Theory Techn.*, Vol. 50, N. 3, March 2002, pp. 814–826.
- [15] F.H. Raab, 'Average efficiency of power amplifiers,' Proceedings of RF Technology Expo, Anaheim, CA, Jan.-Feb. 1986, pp. 474–486.
- [16] S.L. Bussgang, L. Ehrman, J.W. Graham, 'Analysis of nonlinear systems with multiple inputs,' *Proc. IEEE*, Vol. 62, N. 8, Aug. 1974, pp. 1088–1119.
- [17] R.A. Minasian, 'Intermodulation distortion analysis of MESFET amplifiers using Volterra series representation', *IEEE Trans. Microwave Theory Techn.*, Vol. 28, N. 1, Jan. 1980, pp. 1–8.
- [18] P. Colantonio, F. Giannini, E. Limiti, A. Nanni, 'Distortion sideband asymmetries in power amplifiers through Volterra series,' Proceedings of the INMMIC Workshop, Rome, Italy, Nov. 2004, pp. 147–150.
- [19] P. Colantonio, F. Giannini, E. Limiti, A. Nanni, V. Camarchia, V. Teppati, M. Pirola, 'Design approach to improve linearity and power performance of HFET,' *Intern. J. RF Microwave Computer-Aided Engng*, Vol. 18, N. 6, Nov. 2008, pp. 527–535.
- [20] J.C. Pedro, N.B. Carvalho, 'On the use of multi-tone techniques for assessing RF components' iintermodulation properties,' *IEEE Trans. Microwave Theory Techn.*, Vol. 47, N. 12, Dec. 1999, pp. 2393–2402.
- [21] J.C. Pedro, N.B. Carvalho, *Intermodulation Distortion in Microwave and Wireless Circuits*, Norwood, MA, Artech House, 2003.
- [22] N.B. Carvalho, J.C. Pedro, 'Compact formulas to relate ACPR and NPR to two-tone IMR and IP3', *Microwave J.*, Vol. 42, N. 12, Dec. 1999, pp. 70–84.
- [23] P. Kenington, *High Linearity RF Amplifier Design*, Norwood, MA, Artech House, 2000.
- [24] J.A. Piero, 'Characterisation of power amplifiers using noise loading,' Proceedings of ELECTRO '96, 30 April-2 May 1996; pp. 303–308.
- [25] J.C. Pedro, N.B. Carvalho, 'Evaluating co-channel distortion ratio in microwave power amplifiers,' *IEEE Trans. Microwave Theory Techn.*, Vol. 49, N. 10, Oct. 2001, pp. 1777–1784.
- [26] J.C. Pedro, N.B. Carvalho, 'A novel set-up for co-channel distortion ratio evaluation,' *IEEE MTT-S Intern. Microwave Symp. Dig.*, Boston, USA, June 2000, pp. 1854–1854.
- [27] R. Hassun, M. Flaherty, R. Matreci, M. Taylor, 'Effective evaluation of link quality using error vector magnitude techniques,' Proceedings of Wireless Communications Conference, Aug. 1997, pp. 89–94.
- [28] T.T. Ha, *Solid-State Microwave Amplifier Design*, New York, NY, John Wiley & Sons, Ltd, 1981.
- [29] I. Bahl, P. Bhartia, *Microwave Solid State Circuit Design*, New York, NY, John Wiley & Sons, Ltd, 1988.
- [30] R.J. Weber, *Introduction to Microwave Circuits*, Piscataway, NJ, IEEE Press, 2001.
- [31] R.S. Symons, 'Modern microwave power sources,' *IEEE Aerospace Electron. Syst. Mag.*, Vol. 17, N. 1, Jan. 2002, pp. 19–26.
- [32] F. Murgadella, F. Payen, P. Coulon, 'SSPAs & TWTAs: an evolutive situation for electronic warfare applications,' 23rd Annual Technical Digest Gallium Arsenide Integrated Circuit (GaAs IC) Symposium, 2001, Oct. 2001, pp. 149–152.
- [33] F. Murgadella, P. Coulon, C. Moreau, 'Comparisons of technologies and MMICS results for military needs,' 23rd Annual Technical Digest Gallium Arsenide Integrated Circuit (GaAs IC) Symposium, 2001, Oct. 2001, pp. 223–227.
- [34] R.K. Parker, R.H. Abrams, B.G. Danly, B. Levush, 'Vacuum electronics,' *IEEE Trans. Microwave Theory Techn.*, Vol. 50, N. 3, Mar 2002, pp. 835–845.
- [35] J.M. Anderson, 'History and reflections on the way things were - Irving Langmuir and the origins of electronics,' *IEEE Power Engng Rev.*, Vol. 22, N. 3, March 2002, pp. 38–39.
- [36] J.F. Ramsay, 'Microwave antenna and waveguide techniques before 1900,' *Proc. IRE*, Vol. 46, Feb. 1958, pp. 405–414.
- [37] H. Hertz, *Electric Waves*, New York, Macmillan, 1893.
- [38] T.K. Sarka, D.L. Sengupta, 'An appreciation of J.C. Bose's pioneering work in millimeter waves,' *IEEE Antennas Propagat. Mag.*, Vol. 39, N. 5, Oct. 1997, pp. 55–62.
- [39] R.H. Varian, S.F. Varian, 'A high frequency oscillator and amplifier,' *J. Appl. Phys.*, Vol. 10, May 1939, pp. 321–327.
- [40] S. Nakajima, 'The history of Japanese radar development to 1945,' in *Radar Development to 1945*, R. Burns, Ed. Stevenage, UK, Peregrinus, 1988, ch. 18, pp. 243–258.

46 HIGH EFFICIENCY SOLID STATE POWER AMPLIFIERS

- [41] M. Chodorow, E.L. Ginzton, I.R. Nielson, S. Sonkin, 'Design and performance of a high-power pulsed klystron,' *Proc. IRE*, Vol. 41, Nov. 1953, pp. 1584–1602.
- [42] O.M. Stuetzer, 'A crystal amplifier with high input impedance,' *Proc. IRE*, Vol. 38, Aug. 1950, p. 868–871.
- [43] W. Shockley, 'A unipolar 'field-effect' transistor,' *Proc. IRE*, Vol. 40, Nov. 1952, p. 1365–1376.
- [44] T. Mimura, S. Hiyamizuk, T. Fujii, K. Nanbu, 'A new field effect transistor with selectively doped GaAs/n–AlGaAs heterostructures,' *J. Appl. Phys.*, Vol. 19, 1980, pp. L225–L227.
- [45] W.P. Dumke, J.M. Woodall, V.L. Rideout, 'GaAs–GaAlAs heterojunction transistor for high frequency operation,' *Solid State Electron.*, Vol. 15, Dec. 1972, pp. 1339–1334.
- [46] P.M. Asbeck, D.L. Miller, W.C. Petersen, C.G. Kirkpatrick, 'GaAs/GaAlAs heterojunction bipolar transistors with cutoff frequencies above 10 GHz,' *IEEE Electron Device Lett.*, Vol. 3, N. 12, Dec. 1982, pp. 366–368.
- [47] H. Kroemer, 'Theory of a wide-gap emitter for transistors,' *Proc. IRE*, Vol. 45, Nov. 1957, pp. 1535–1537.
- [48] <http://mitsubishichips.com/products/wave>
- [49] <http://www.fcsi.fujitsu.com>
- [50] V.L. Granatstein, R.K. Parker, C.M. Armstrong, 'Vacuum electronics at the dawn of the twenty-first century,' *Proc. IEEE*, Vol. 87, N. 5, May 1999, pp. 702–716.
- [51] R.J. Trew, J.-B. Yan, P.M. Mock, 'The potential of diamond and SiC electronic devices for microwave and millimeter-wave power applications,' *Proc. IEEE*, Vol. 79, N. 5, May 1991, pp. 598–620.
- [52] C.M. Johnson, N.G. Wright, M.J. Uren, K.P. Hilton, M. Rahimo, D.A. Hinchley, A.P. Knights, D.J. Morrison, A.B. Horsfall, S. Ortoland, A.G. O'Neill, 'Recent progress and current issues in SiC semiconductor devices for power applications,' *IEE Proc. Circuits, Devices Syst.*, Vol. 148, N. 2, April 2001, pp. 101–108.
- [53] C. Lee, P. Saunier, Yang Jinwei, M.A. Khan, 'AlGaIn–GaIn HEMTs on SiC with CW power performance of >4 W/mm and 23% PAE at 35 GHz,' *IEEE Electron Device Lett.*, Vol. 24, N. 10, Oct. 2003, pp. 616–618.
- [54] C. Lee, Yang Jinwei, M.A. Khan, P. Saunier, 'Ka-band CW power performance by AlGaIn/GaIn HEMTs on SiC,' 2003 Device Research Conference, June 2003, pp. 17–18.
- [55] U.K. Mishra, P. Parikh, Yi-Feng Wu, 'AlGaIn/GaIn HEMTs – An overview of device operation and applications,' *Proc. IEEE*, Vol. 90, N. 6, June 2002, pp. 1022–1031.
- [56] G.G.I. Haddad, R.J. Trew, 'Microwave solid-state active devices,' *IEEE Trans. Microwave Theory Techn.*, Vol. 50, N. 3, March 2002, pp. 760–779.
- [57] J.L.B. Walker, *High Power GaAs FET Amplifiers*, Norwood, MA, Artech House, 1993.
- [58] D. Pavlidis, 'HBT vs. PHEMT vs. MESFET: What's best and why,' *Compound Semicond.*, Vol. 5, N. 5, 1999, pp. 56–59.
- [59] S.M. Sze, *Semiconductor Devices Physics and Technology*, New York, John Wiley & Sons, Ltd, 2001.
- [60] M. Golio, *RF and Microwave Semiconductor Device Handbook*, Boca Raton, CRC Press, 2003.
- [61] M.A. Khan, G. Simin, S.G. Pytel, A. Monti, E. Santi, J.L. Hudgins, 'New developments in gallium nitride and the impact on power electronics,' *IEEE 36th Power Electronics Specialists Conference, PESC'05*, 2005, pp. 15–26.
- [62] U.K. Mishra, L. Shen, T.E. Kazior, W. Yi-Feng, 'GaN-based RF power devices and amplifiers,' *Proc. IEEE*, Vol. 96, N. 2, Feb. 2008, pp. 287–305.
- [63] O. Berger, 'GaAs MESFET, HEMT and HBT competition with advanced Si RF technologies,' International Conference on Compound Semiconductor Manufacturing Technology, ManTech 1999, 4 pages.
- [64] F.H. Raab, P. Asbeck, S. Cripps, P.B. Kenington, Z.B. Popovic, N. Potheary, J.F. Sevic, N.O. Sokal, 'RF and microwave power amplifier and transmitter technologies. Part I,' *High Frequ. Electron.*, Vol. 2, N. 3, May 2003, pp. 22–36.
- [65] D.J. Friedman, M. Meghelli, B.D. Parker, J. Yang, H.A. Ainspan, A.V. Rylyakov, H.Y. Kwark, M.B. Ritter, L. Shan, S.J. Zier, M. Sorna, M. Soyuer, 'SiGe BiCMOS integrated circuits for high-speed serial communication links,' *IBM J. Res. Dev.*, Vol. 47, N. 2/3, March/May 2003, pp. 259–282.
- [66] L.E. Larson, 'SiGe HBT BiCMOS technology as an enabler for next generation communications systems,' Proceedings of 12th GAAS Symposium, Amsterdam (NL), Oct. 2004, pp. 251–254.
- [67] A.K. Oki, D.C. Streit, D.K. Umamoto, L.T. Tran, K.W. Kobayashi, F.M. Yamada, P.C. Grossman, T. Block, M.D. Lammert, S.R. Olson, J. Cowles, M.M. Hoppe, L. Yang, A. Gutierrez-Aitken, R.S. Kagiwada, S. Nojima, E.A. Rezek, W. Pratt, J. Neal, P. Seymour, V. Steel, 'Future trends of HBT technology for commercial and defense applications,' *IEEE MTT-S Symposium on Technologies for Wireless Applications Dig.*, Feb. 1997, pp. 123–125.

- [68] K.J. Fischer, K. Shenai, 'Effect of bipolar turn-on on the static current-voltage characteristics of scaled vertical power DMOSFET's,' *IEEE Trans. Electron. Devices*, Vol. 42, N. 3, March 1995, pp. 555–563.
- [69] G. Doudorov, 'Evaluation of Si-LDMOS transistor for RF power amplifier in 2–6 GHz frequency range,' Masters Thesis, Linköping University, Sweden, June 2003.
- [70] L. Vestling, B. Edholm, J. Olsson, S. Tiensuu, A. Soderbarg, 'A novel high-frequency high-voltage transistor using an extended gate RESURF technology,' *IEEE International Symposium on Power Semiconductor Devices and IC's*, ISPSD'97, May 1997, pp. 45–48.
- [71] J. Olsson, N. Rorsman, L. Vestling, C. Fager, J. Ankarcrone, H. Zirath, K.-H. Eklund, '1 W/mm RF power density at 3.2 GHz for a dual-layer RESURF LDMOS transistor,' *IEEE Electron. Device Lett.*, Vol. 23, N. 4, April 2002, pp. 206–208.
- [72] G.W. Taylor, R.J. Bayruns, 'A comparison of Si MOSFET and GaAs MESFET enhancement/depletion logic performance,' *IEEE Trans. Electron Devices*, Vol. 32, N. 9, Sept. 1985, pp. 1633–1641.
- [73] A.P. Zhang, L.B. Rowland, E.B. Kaminsky, J.W. Kretchmer, R.A. Beaupre, J.L. Garrett, J.B. Tucker, 'Microwave power SiC MESFETs and GaN HEMTs,' *Proceedings of IEEE Lester Eastman Conference on High Performance Devices*, Aug. 2002, pp. 181–185.
- [74] R.A. Sadler, S.T. Allen, W.L. Pribble, T.S. Alcorn, 'SiC MESFET hybrid amplifier with 30 W output power at 10 GHz,' *Proceedings of IEEE Cornell Conference on High Performance Devices*, Aug. 2000, pp. 173–177.
- [75] C. Lanzieri, 'Devices and technologies for power amplifiers', Short Course on High Efficiency Power Amplifier Design. Gallium Arsenide Applications Symposium, London, 2001.
- [76] M. Golio, *Microwave MESFETs and HEMTs*, Norwood, MA, Artech House, 1991.
- [77] F. Schwierz, 'Microwave transistors: the last 20 years,' *Proceedings of IEEE Third International Caracas Conference on Devices, Circuits and Systems*, March 2000, pp. D28/1–D28/7.
- [78] H. Wang, G.S. Dow, B.R. Allen, T.-N. Ton, K.L. Tan, K.W. Chang, T.-h. Chen, J. Berenz, T.S. Lin, P.-H. Liu, D.C. Streit, S.B. Bui, J.J. Raggio, P.D. Chow, 'High-performance in W-band monolithic pseudomorphic InGaAs HEMT LNA's and design/analysis methodology,' *IEEE Trans. Microwave Theory Techn.*, Vol. 40, N. 3, March 1992, pp. 417–428.
- [79] M. Zaknoute, Y. Cordier, S. Bollaert, D. Ferre, D. Theron, Y. Crosnier, '0.1 μm high performance metamorphic In_{0.32}Al_{0.68}As/In_{0.33}Ga_{0.67}As HEMT on GaAs using inverse step InAlAs buffer,' *IEEE Electron. Lett.*, Vol. 35, N. 19, Sept. 1999, pp. 1670–1671.
- [80] C.S. Whelan, P.F. Marsh, W.E. Hoke, R.A. McTaggart, C.P. McCarroll, T.E. Kazior, et al., 'GaAs metamorphic HEMT (MHEMT): an attractive alternative to InP HEMTs for high performance low noise and power applications,' *Proceedings of International Conference on Indium Phosphide and Related Materials*, May 2000, pp. 337–340.
- [81] F. Schwierz, J.J. Liou, *Modern Microwave Transistors. Theory, Design, and Performance*, New York, John Wiley & Sons, Ltd, April 2003.
- [82] R.S. Pengelly, 'Improving the linearity and efficiency of RF power amplifiers,' *High Freq. Electron.*, Vol. 1, N. 5, Sept. 2002, pp. 26–34.

